Università degli Studi di Ferrara

DOCTORAL COURSE IN
"MEDICINA MOLECOLARE"

CYCLE XXXVII

COORDINATOR Prof. Pinton Paolo

SERCA MODULATION REVERSES GLUCOCORTICOID RESISTANCE IN *NOTCH1*-MUTATED T-CELL ACUTE LYMPHOBLASTIC LEUKEMIA

Scientific/Disciplinary Sector (SDS) MED/15

Candidate

Dott.ssa Vento Federica

Supervisor

Prof. Cuneo Antonio

Co-Supervisor

Prof. Roti Giovanni

Years 2021/2024

INDEX

1. INTRODUCTION

1.1. T-cell Acute Lymphoblastic Leukemia

T-cell acute lymphoblastic leukemia (T-ALL) is an aggressive hematological malignancy characterized by the accumulation of lymphoblast in the bone marrow (BM) and peripheral blood (PB) and consequent high tumor burden and highly proliferating malignant lymphoid cells (1,2). It is frequently linked to acquired chromosomal translocations as well as other genetic and epigenetic abnormalities that result in the aberrant expression of a specific subset of transcription factors (3).

The accelerated tumor growth may reflect in part the capacity of immature thymocytes to divide at high rates in critical steps during early T-cell development and it is fueled by the activation of specific oncogenic pathways (4).

From a physiological point of view, during normal T-cell development, early T-cell precursors enter the thymus at the cortical-medullary junction, where they are exposed to the thymic microenvironment's instructional signals, which predominantly stimulate interleukin-7 (IL-7) and stem cell factor to promote cell development and proliferation. The earliest T-cell lineage committed precursor cell is the immature CD34+ cell that has just entered the thymus and can differentiate, through various intermediate subsets, into mature T-cells carrying a functional T-cell receptor (TCR) from the TCRab or TCRgd lineage (4,5).

The malignant counterpart occurs when biological processes such as differentiation, self-renewal capacity, proliferation, and apoptosis are targeted and altered by several types of neoplasia-associated genetic alteration such as translocations, deletions, and mutations of genes that encode for proteins involved in signaling transduction, epigenetic regulation, and transcription (6). This process causes an uncontrolled clonal expansion resulting in the development of T-ALL (7).

In T-ALL, the malignant clone proliferates and spreads throughout the body, starting from the BM to the PB, lymph nodes and eventually the central nervous system (CNS) and other organs. The lymphoblasts spreading causes the T-ALL symptoms and signs, such as bone pain, leucocytosis, fatigue, and neurological symptoms. Therefore, the expansion of immature lymphoblasts in the BM represses hematopoiesis, resulting in a deficiency of normal PB cells with consequent cytopenia (8).

T-ALL counts approximately 15-20% of all ALLs with a different distribution between adult and childhood, comprising 10-15% of pediatric and 25% of adult primary ALL cases, respectively (9). It occurs most frequently in children with a peak incidence between 2 and 5 years of age and is one of the most common childhood malignancies (10). Overall cure rates are reaching over 75% in children and 50% in adult T-ALL cases. Current treatment regimens include risk-adapted high-dose chemotherapy, hematopoietic stem-cell transplantation, and supportive care. Unfortunately, T-ALL patients often relapse quite early during treatment resulting in a 5 year survival rate of 7-23% in relapsed T-ALL (5). Nevertheless, the use of new pediatric-oriented protocols in adult settings and intensified treatments, based on the persistence of minimal residual disease (MRD) in children and adults, have greatly improved patient outcomes (11). Despite the introduction of hematopoietic stem cell transplantations for refractory leukemias, the clinical outcome of these high-risk, primary resistant tumors remains extremely unfavorable (12).

The evolution of flow cytometry analysis has allowed the clear definition of T-lineage and stage of differentiations of malignant lymphoproliferative disorders. According to European Group for the Immunological characterization of Leukaemias (EGIL), recognized T-ALL subsets are the following: pro-T (cCD3+, CD7+), pre-T (cCD3+, CD7+ and CD5/CD2+), cortical T (cCD3+, Cd1a+, sCD3+/−) and mature-T (cCD3+, sCD3+, CD1a−). Finally, a novel subgroup that was recently characterized is represented by the so called ETP-ALL (Early T-

cell Precursor), which shows specific immunophenotypic features, such as the lack of CD1a and CD8 expression, weak CD5 expression, and expression of at least one myeloid and/or stem cell marker (7,13). The positivity of CD5 in an early T-cell precursor phenotype identifies the near-ETP subgroup (14).

1.2. Genetics of T-cell Acute lymphoblastic Leukemia

T-ALL has a highly varied genetic background due to any oncogenes and onco-suppressors linked to leukemia's beginning and advancement, frequently by intersecting on a few key cellular processes (11).

Abnormalities in T-ALL can be divided into two different subgroups, type A and type B, according to specific gene expression signatures and aberrant activation of specific T-ALL transcription factor oncogenes. Type A abnormalities cause the up-regulation of oncogenes encoding for transcriptional factors critical in T-cell development, maturation, and differentiation. At least 70% of T-ALL cases can be classified into different genetic subgroups, based on the expression of specific transcription factor oncogenic drivers and hierarchical clustering of gene expression data. These transcriptional regulators include the basic helix-loop-helix transcriptional factor genes TAL1, TAL2, TLX1, TLX3, NKX2-1, NKX2-2; the LIM only domain genes LMO1 and LMO2 and HOXA homeobox genes (7,15).

Genes that code for many protein families, including signal pathway proteins, ribosomal proteins, tyrosine kinases, and epigenetic factors, are involved in type B abnormalities. Such T-ALL genetic groups are distributed differently in adults and children. For instance, HOXA-positive T-ALL has an immature or ETP phenotype in 40–45% of cases; in ETP-ALL, leukemic blasts depend on the anti-apoptotic protein BCL2, which is widely overexpressed in this subtype of T-ALL. HOXA subgroup is also characterized by aberrant DNA replication and cell cycle due to deletion of cell cycle regulators, such as *CDKN2AB* (85%) or *CDKN1B*

(25%) (16). On the other hand, NKX2-1-positive cases show a high rate of deletions of *LEF1*, a DNA-binding transcription factor, and a high rate of mutations of *RPL10*, a ribosomal protein. Additionally, TLX3 and TLX1, which belong to the NKL family of homeobox transcription, are expressed in 40% of T-ALL, sharing common oncogenic pathways (15).

TAL1 subgroup counts for 30-45% of pediatric and 10-15% of adult T-ALL (17). It shows frequently chromosomal rearrangements, or noncoding sequence mutations, which cause the activation of members of the basic helix-loop-helix family of transcription factors (TAL1 and TAL2) or the LIM-only domain (LMO1, LMO2, and LMO3) proteins (18). TAL and LMO proteins belong to the same transcriptional complex and are frequently co-deregulated in T-ALL, suggesting a cooperative role in T-leukemogenesis (11).

Generally, T-ALL is frequently characterized by chromosomal abnormalities, such as deletions at the *CDKN2A*/*CDKN2B* tumor suppressor locus on the short arm (p) of chromosome 9, resulting in *CDKN2A*/*CDKN2B* inactivation and translocation affecting the *TCR* genes (19,20). Additional mutations include loss-of-function alterations of hematopoietic transcription factor genes, including *BCL11B*, *ETV6*, *GATA3*, *LEF1*, *RUNX1* and *WT1* (20,21). Several genes that encode epigenetic regulators and chromatin modifiers are also mutated in T-ALL, including *EED*, *EZH2* and *SUZ12*, which encode core components of Polycomb repressor complex 2 (PRC2) (21,22). Several additional intracellular signaling pathways are activated by mutation, including the Pi3k–Akt–mTor pathway, most affected by *PTEN* deletion (23,24); the Jak-Stat pathway through activating mutations in the interleukin 7 receptor α-chain gene (IL-7Rα) (25,26); Ras–Mapk signaling through *KRAS* and *NF1* mutation (21). Furthermore, constitutive activation of the *NOTCH1* gene plays a key role in T-cell transformation and is implicated in the pathogenesis of 50-70% T- ALL. *NOTCH1* is considered a driver gene, target of mutations in the

heterodimerization domain (HD) or the peptide sequence rich in proline, glutamate, serine and threonine domain (PEST) (27,28).

The Notch1 pathway plays a fundamental role in T cell functions like stem cell self-renewal, proliferation, and differentiation in the thymus. Consequently, its dysregulation in downstream pathways, such as MYC signaling or PTEN–AKT signaling, can lead to leukemic transformation or metabolic dysregulation (4,29).

1.3. NOTCH

1.3.1. NOTCH Structure and Signaling

In mammals, the “NOTCH family” comprises a group of four transmembrane receptor proteins (NOTCH1-4) that interact with ligands expressed in contacting cells (30). Structurally, NOTCH receptors consist of a modular structure that is composed of different functional regions: an extracellular domain (N-ECD) at the N-terminal, a transmembrane domain (N-TM), and a NOTCH intracellular domain (N-ICD) at the C-terminal. The *NOTCH1* gene is where most of the recurring somatic mutations of all NOTCH proteins (I-IV) were found. More specifically, human N1-ECD contains 36 homologous epidermal growth factor (EGF)-like tandem repeats and three Lin-12/Notch units (LNR). Adjacent to the LNR domain lies the juxta-membrane (JME) and heterodimerization domain (HD), the linker between the N1-ECD and N1-ICD. N1-ICD consists of a membrane-proximal RBPJ-associated molecule (RAM) region, seven ankyrin-like repeats (ANK) and a C-terminal transactivation domain (TAD) that harbors the nuclear localization signal (NLS) (19).

The NOTCH1 maturation steps start in the *trans*-Golgi with the proteolytic processing by a furin-like convertase at the site “S1” that lies 70 amino acids external to the transmembrane domain, yielding two non-covalently associated extracellular (N-ECD) and transmembrane (N-TM) subunits (27). Once preprocessed in the ER/Golgi, NOTCH1 receptors migrate to

the cell membrane and interact with the ligand. The subsequent binding with ligands induces a conformational change that allows two subsequent proteolytic cleavages on the N-TM subunit. The first cleavage (S2) is mediated by zinc-dependent disintegrin and metalloprotease (ADAM10/TACE) and occurs within the NOTCH JME domain, proximal to the N-TM (31,32). S2 cleavage results in a transient intermediate recognized by the -secretase complex, which mediates the second cleavage (S3) within the transmembrane domain (33–35). The γ-secretase complex is a membrane-embedded protease complex composed of four proteins: presenilin (PSEN1 or PSEN2), presenilin enhancer-2 (PEN-2), anterior pharynx defective-1 (APH-1), and nicastrin (NCSTN) (28). Nicastrin recognizes transient intermediate through its amino terminus and PSEN is necessary for the catalytic activity, which releases N-ICD. Finally, N-ICD is translocated into the nucleus and interacts with a transcription-activating complex in which the RAM and ANK N-ICD motifs bind the DNA factor suppressor of hairless (Lag-1 or CSL) and recruit the N-terminal helices of mastermind-like (MAML) family co-activator (36). In succession, MAML recruits the histone acetyl-transferases (p300/CBP) to induce the transcription of downstream genes, such as *HES*, *HEY*, and *MYC* (37).

Notch physiologically regulates several cellular networks, from embryogenesis to adult tissue commitment and homeostasis, to differentiation of T-cells. Depending on the cellular context, *NOTCH* may act as an oncogene or tumor suppressor but, more importantly, the degree of its contribution to the disease depends on the presence of activating or suppressing genetic aberrancies. Gain-of-function *NOTCH1* mutations are sequenced in 50–70% of T-ALL cases, in 10–15% of chronic lymphocytic leukemia (CLL) and mantle cell lymphoma (MCL) and a subset of diffuse large B cell lymphoma (DLBCL) (37). The discovery of the oncogenic role of *NOTCH* in T-ALL anticipated the identification of *NOTCH*

aberrations in solid tumors, such as lung adenocarcinoma, medulloblastoma, melanoma, colon cancer, and more frequently, in breast cancer (38).

1.3.2. Anti-NOTCH1 Therapies: Challenges and Advances

The preponderance of oncogenic *NOTCH1* mutations in lymphoid malignancies has prompted the search for effective anti-NOTCH1 therapeutics. Because Notch activation relies on γ-secretase-mediated proteolysis, γ-secretase inhibitors (GSIs) have been studied for T-ALL treatment (39,40). GSIs are small molecules that can effectively suppress Notch signaling by blocking intramembrane proteolytic processing of NOTCH1 by the γ-secretase complex. However, the first generations of GSIs were poorly tolerated due to on-target gastrointestinal toxicity. The toxic effect of GSIs is a consequence of the lack of substrate specificity of these molecules resulting in the combined inhibition of wild-type NOTCH1 and NOTCH2 in intestinal progenitor cells. GSI treatment resulted in cell cycle arrest and accumulation of goblet cells in the gut mediated by upregulation of the gene encoding the transcription factor Kruppel-like factor-4 (Klf4), a negative regulator of the cell cycle required for goblet cell differentiation. Recently, several studies have identified a second generation of GSIs with better tolerability profiles and combination strategy to overcome the limitation showed with the single drug treatment (27). Importantly, this combination strategy considers GCs, the first drug classes used in clinic for the treatment of patients with T-ALL. Real and colleagues demonstrated that combining GSIs with GCs improved the anti-leukemic effects of GSIs and reduced their gastrointestinal toxicity *in vivo* compared to treatment with GSI alone. GSIs sensitize steroid resistant T-ALL cell lines to GCs therapy and induce apoptosis through induction of apoptotic initiator, *BCL2L11*. On the other hand, steroids mediate the induction of cyclin D2 (Ccnd2), a cyclin associated with cell cycle progression, which induces the down regulations of Klf4. These results highlight the functional relevance

of *CCND2* upregulation induced by steroids treatment for the protection from GSI-induced toxicity in the gut and support the development of innovative anti-NOTCH1 therapies (27).

Because of the therapeutic challenges of GSI therapy, different strategies were studied to inhibit NOTCH1, such as the development of NOTCH1-directed antibodies (Ab) that block Notch ligand-receptor interaction. Different research groups developed a class of receptor-directed antibodies, such as monoclonal antibodies (mAb), directed against the EGF-repeat region and directed against the NRR NOTCH1 domain. On the other hand, another class of antibodies to impair NOTCH activation is directed against NOTCH1 ligands such as DLL1 and DLL4. However, the targeting of ligand appears to be an ineffective strategy in the context of ligand independent *NOTCH1* mutations in T-ALL (37). Additionally, it has been developed an alternative approach to modulate the NOTCH1 transcription factor complex using for example SAHM1, a stabilized a-helical peptide that interferes directly with the recruitment of MAML1 into the NOTCH-RBPJ transactivation complex (37).

The Notch signaling pathway plays a significant role in the pathogenesis of human cancers. Notch controls both cell-intrinsic and extrinsic circuits leading to tumor development, progression and response to therapy. Several therapeutic efforts have historically focused on modulating Notch signaling by using small molecules such as GSI or antibody-based strategies. However, these approaches have a poor therapeutic window - wild type vs mutant proteins - limiting their application in human diseases. This is not the case of small molecules targeting the sarco-endoplasmic reticulum Ca^{2+}-ATPase (SERCA) (27). SERCA inhibition interferes with Notch trafficking and its activation, emerging as druggable approach for *NOTCH*-dependent cancers.

Gain-of-function *NOTCH1* mutations, found in over 60% of T-cell Acute Lymphoblastic Leukemia (T-ALL) cases, drive leukemia development (41,42). Thus, targeting aberrant NOTCH1 activity with anti-Notch drugs is a promising and long-waited strategy (29).

1.4. SERCA

1.4.1. SERCA Structure and Function

SERCA (Sarco-Endoplasmic Reticulum Ca^{2+} ATPase) protein, located in the sarco-endoplasmic reticulum (ER), belongs to the superfamily of active transporters known as P-type ATPases. There are three genes *ATP2A1* (16p11.2), *ATP2A2* (12q24.11), *ATP2A3* (17p13.2) that encode for SERCA1, SERCA2 and SERCA3, respectively (43). Currently, over 70 SERCA isoforms resulting from alternative splicing are deposited in the Protein Data Bank database.

SERCA proteins have the function of maintaining intracellular Ca^{2+} homeostasis by pumping Ca^{2+} from the cytosol into the ER. These 110 KDa pumps are organized in 10 transmembrane (TM), helices (M1-M10) along with two Ca^{2+} binding site (site I and II), a small luminal tail and three cytoplasmic domains (44). The enzymatic reaction, proposed as the Post-Albers scheme, alternates phases with high ($2Ca^{2+}$E1) or low (E2) affinity to Ca^{2+} coupled with high ($2Ca^{2+}$E1 ~ P) or low (E2 ~ P) energy phosphorylated states (45). SERCA proteins have been involved in several human diseases from inherited syndrome to heart failure. For instance, loss-of-function mutations of *ATP2A1* cause Brody myopathy, similarly *ATP2A2* mutations account for the development of the Darier disease (keratosis follicularis), a severe skin disorder (46). Given its role in Ca^{2+} homeostasis and its effect on cell survival and ER stress pathway, the potential involvement of SERCA in cancer progression has been an active area of investigation. Some studies have demonstrated the involvement of genetic alterations of the *ATP2A2* gene in tumor development (46–48).

1.4.2. Targeting NOTCH1 with SERCA Inhibitors: Mechanisms and Therapeutic Potential

Several studies described that the trafficking events leading to a correct NOTCH activation may be disrupted in the presence of a defective Ca^{2+}-ATPase function in a Drosophila model

(49). Loss of function alleles of the Drosophila SERCA homologous gene *CA-P60A* alters proper synthesis, folding, and trafficking of the NOTCH receptor in the ER/Golgi compartments. Consistently, in Drosophila S2 cultured lines, the treatment with general SERCA inhibitors such as TG and cyclopiazonic acid (CPA) primarily reduces the number of NOTCH proteins that reach the cell surface (49). In line with these findings, as mentioned above, from a study of Roti et al. SERCA emerged as a novel potential therapeutic target in *NOTCH1*-associated cancers. They performed a gene expression-based high-throughput screening (GE-HTS) to identify inhibitors of oncogenic *NOTCH1* signatures or enhancers of *NOTCH1* HD mutant L1601PΔP activity in T-ALL. Among the top cDNA hits, the Ca^{2+} pump P-type ATPase SERCA was identified as a gatekeeper of oncogenic *NOTCH1* and in parallel, one of the top compound hits identified was TG which is a non-competitive inhibitor of SERCA. TG induced a *NOTCH1*-off signature in a dose-dependent fashion in *NOTCH1* mutant T-ALL cells and reduced the expression of the direct Notch1 target genes *MYC*, *HES1* and *DTX1.* Furthermore, NOTCH1 inhibition resulted in G0/G1 arrest in human T-ALL cells and reduced T-ALL formation in an *in vivo* model (3,49). TG is a potent natural product isolated from the umbelliferous *Thapsia garganica* plant that irreversibly stabilizes SERCA in an inactive state with low Ca^{2+} affinity (E2-Ca^{2+} free conformation), inhibiting both ATPase and Ca^{2+} transport activity. With varying selectivity, TG binds to all SERCA isoforms in the transmembrane helices M3 (at Phe256), M5 (at Ile765), and M7 (at Tyr837). Due to the strong dependence of mutated NOTCH1 to ER Ca^{2+} for correct folding, TG exerts a preferential activity against mutated NOTCH1 proteins, as shown by its antileukemic effect and the lack of gastrointestinal toxicity in a human T-ALL xenograft model, in sharp contrast with previous experiences with GSI (50,51). However, translating the effects of TG into a clinical setting could be challenging: first, it's a natural compound and it eventually requires a synthesis process of more than 10 steps; furthermore, TG displays a generic effect towards all SERCA isoforms, particularly on the cardiac isoform SERCA2a. TG binding to

SERCA results in an increase in cytosolic Ca^{2+} concentration and a depletion of Ca^{2+} stored in the ER, thus the delivery of free TG to humans might cause cardiac toxicity due to a calcium ion shift (47,52). Initially, one way to overcome these limitations and to improve TG delivery to cancer cells was based on a pro-drug approach. For instance, the TG derivative mipsagargin/G202 is coupled with a masking peptide cleaved by the carboxypeptidase prostate-specific membrane antigen (PSMA) that is overexpressed in the neovasculature of several tumors including hepatocellular carcinoma, mesothelioma, ovarian, bladder, renal, and breast cancer. This peptide reduces the affinity of these molecules toward SERCA in non-neoplastic cells. Therefore, when mipsagargin intercepts PSMA on tumor cells or neoplastic neoangiogenic vessels, it is cleaved into a cytotoxic analog of TG (12-ADT-Asp) and diffuse specifically into cancer cells (53). In line with this type of enzymatic-based approach, Roti and collaborators have coupled TG with other molecules such as folic acid (FA), exploiting the dependency of T-ALL on folic acid metabolism due to the higher expression of folate receptor 2 (FR-2) in T-ALL cells compared to the normal counterpart (54). Next, they showed that the conjugable alcohol derivative of TG, 8-*O*-debutanoyl-thapsigargin, inhibits NOTCH1 in a way that is similar to the effect of TG observed in T-ALL models. Notably, 8-*O*-debutanoyl-thapsigargin preserved a selective activity against mutant over *NOTCH1* wild-type T-ALL. Subsequently, they connected the carboxylate of folic acid to the C8-alcohol of 8-*O*-debutanoyl-thapsigargin via a cleavable ester linkage to generate JQ-FT. JQ-FT was 150 times more tolerable in mice than unconjugated TG and exerted an anti-leukemic effect in a preclinical *NOTCH1* mutated T-ALL *in vivo* model (54).

Another strategy to overcome the TG limitations due to cardiac effects is to search for novel isoform-specific SERCA inhibitors that share a therapeutic index similar to that of TG, but which have a safer toxicity profile. Beyond the few SERCA inhibitors, the tricyclic clerodane diterpene Casearin J (CJ) was extensively explored as a NOTCH1 inhibitor in T-ALLs for its

capacity to decrease the cell surface expression of N1-TM and to prevent the formation of cleaved N1-ICD modules (51). More recently, Marchesini and colleagues completed a small molecule screening of 191,000 compounds active on P-type ATPases and identified CAD204520, a new selective SERCA inhibitor with favorable pharmacodynamic properties. CAD204520,4-[2-[2-[3-propyl-6-(trifluoromethoxy)-1H-indol-2-yl]-1-piperidyl] ethyl]-morpholine dihydrochloride binds SERCA between the transmembrane helices M1, M2, M3, and M4 through two polar interactions with Asp59 on M1 and Asn101 on M2, as well as through some hydrophobic interactions with Leu61, Val62, Ile307, Pro308, and Pro312. Although this binding groove is different from that of TG, CAD204520 still maintains anti-*NOTCH1* mutated leukemia properties both in preclinical and *in vivo* models, without disrupting Ca^{2+} homeostasis and cardiac toxicity. To further explore the pharmacodynamics of CAD204520, they generated a human T-ALL cell line (ALL/SIL) resistant to the effect of TG (R) by exposing the cells to increased concentrations of TG. Whole exome sequencing analysis identified a missense single-nucleotide polymorphism in the *ATP2A2* locus mapping between the Asp254 and Leu260 amino acids lying in the third transmembrane helix (M3) of SERCA2 causing a glycine 257 to valine mutation (p.G257V). The introduction of the bulky valine side chain will limit the freedom of movement of the neighboring residue Phe256, which must move to host TG binding, thus providing a potential explanation for the resistance effect to TG. However, in these cells, they showed the lack of cross-resistance with CAD204520, confirmed by the crystallography structure that showed the different binding pocket of the two compounds. These data suggest that early characterization of the binding mechanism may overcome potential relapse from mutant clones (54,55).

1.5. Glucocorticoid Receptor Signaling and Resistance Mechanisms in T-ALL

GC are one of the first drug classes used in clinics for the treatment of patients with ALL (56) and are now used as backbone therapy of almost all the chemotherapy regimens for ALL therapy. They exert their activity by binding to a specific intracellular glucocorticoid receptor (GR), which is a ligand-inducible transcriptional factor encoded by the *NR3C1* gene. In the absence of a specific ligand, GRs remain in the cytoplasm by their association with chaperone proteins, such as Hsp70 and Hsp90 (57). Ligand binding generates a formation of the GC-GR complex, causing conformational changes and translocation to the nucleus, where it binds to accessible chromatin domains containing GC response elements (GRE) at proximal promoter regions or distal sites of a gene to induce chromatin remodeling and activate gene transcription (58). The GR-encoding gene *NR3C1* contains nine exons that can produce various splice isoforms. In humans, the primary GRα isoform encodes a protein of 777 amino acids. In comparison, GRβ results from alternative splicing, producing a truncated protein of 742 amino acids. This truncated variant is unable to bind GCs and regulates a different set of genes from those targeted by GRα. When co-expressed with GRα, GRβ acts as a dominant-negative modulator and has been linked to GC resistance (59).

GCs are widely recognized for their anti-inflammatory and immuno-suppressive activities (60). Many of the most important effects of GCs, however, are their direct actions on T cells, primarily through transcriptional regulation: enhancing the expression of immunomodulatory proteins, inhibitory receptors, and genes that promote apoptosis while reducing the expression of pro-inflammatory cytokines, co-stimulatory molecules, and cell cycle regulators (61,62). GCs, such as dexamethasone and prednisolone, are now essential elements of multi-agent chemotherapy regimens used to treat hematologic malignancies due to their ability to induce apoptosis in lymphocytes. Although GCs are efficient at eliminating malignant lymphoid cells, about 20% of ALL patients still have *de novo* or

acquired resistance, which is a major obstacle to their efficacy (34). Transcriptional responses to GC receptor activation are tissue and context-specific, and the selective proapoptotic response to GR signaling in lymphoid cells depends on their capacity to induce lymphoid-restricted transcriptional upregulation of *BCL2L11*, which encodes the proapoptotic BH3-only factor BIM (63).

GC response is variable among T-ALL patients, and steroid resistance has been observed in a significant fraction of patients during induction therapy. Furthermore, secondary resistance to GC therapy is also common in R/R T-ALL and contributes significantly to therapeutic failure. Additionally, it has been shown that in T-ALL there is a relationship between abnormal activation of specific signaling pathways and steroid response, such as Notch, IL7-R/JAK/STAT, RAS/MEK/ERK, and PTEN/PI3K/AKT/mTOR (64,65). Moreover, it has been demonstrated that GC resistance in ALL is related to different genetic abnormalities, which cause not only upregulation of the above-mentioned pathways but also acceleration of cellular growth and metabolism, downregulation of the proapoptotic proteins, such as BIM, and upregulation of the antiapoptotic proteins, such as BCL-2, BCL-XL, MCL-1, with a consequent apoptosis inhibition and overexpression of multidrug-resistance proteins (66). PI3K-AKT activation plays a major role in the pathogenesis of T-ALL, particularly in leukemias, harboring mutations and deletions in the *PTEN* tumor suppressor gene, AKT1 emerged as a plausible candidate for explaining in part the GC resistance (23). *In silico* studies of signaling pathways, influencing transcriptional patterns linked to GC resistance in T-ALL suggested that AKT1 may phosphorylate the GR at position S134, generating GC resistance (67). This inhibits the nuclear relocalization of the GR protein and prevents the transcriptional control of GC target genes. The inactivation of the GR can lead to resistance to GC therapy, but it should be considered that alternative processes downstream of AKT1 can also do so by enhancing T-ALL cell proliferation, metabolism, and

survival. In this regard, mTOR phosphorylation by AKT impairs GC-induced apoptosis by increasing the expression of MCL-1 anti-apoptotic protein. These data support the role of PTEN/PI3K/AKT/mTOR pathway as a therapeutic target for the reversal of primary GC resistance in T-ALL (67,68).

Furthermore, Lauren K. Meyer et al. support the fact that the presence of IL-7 improves downstream signal transduction, increasing STAT5 transcriptional output and upregulating the pro-survival protein BCL-2, which is sufficient to counteract the proapoptotic effect of GCs (69). Their data therefore suggests that IL-7–induced GC resistance may protect these early thymocyte populations from apoptosis in the presence of endogenous GCs. Furthermore, they demonstrate that this mechanism of intrinsic resistance was retained in T-ALL cells resembling early thymocytes, where it may be exploited to enable resistance to pharmacologic concentrations of GCs (67).

As mentioned above, more than 50% of human T-ALL are known to exhibit *NOTCH1* activating mutation and NOTCH1 is involved in the regulation of *NR3C1* expression and GR protein levels. The underlying mechanism was shown to involve *HES1*, a transcriptional repressor, which is upregulated by Notch1 signaling and binds to *NR3C1* promoters, responsible for the GR autoregulation. NOTCH1 also acts as a positive modulator of the IL-7R that can be also activated by GCs causing their resistance (70). Importantly, while confirming that GC resistance of T-ALL cells requires an unaltered Notch1 signaling, GC treatment reduces NOTCH1 expression in sensitive cell lines, highlighting that any factors that modulate *NR3C1* signaling will also affect NOTCH1 expression and response (54). On the other hand, inhibition of Notch1 signaling enhances GR auto-upregulation and GC sensitivity in otherwise GC-resistant T-ALL cells (45), laying the groundwork for a strict link between mutated Notch1 pathway and reversal of GC resistance.

2. AIM OF THE STUDY

Given its critical oncogenic role in several human cancers, Notch1 signaling has garnered increased attention as a potential therapeutic target. To date, several Notch inhibitors, including GSI, have shown therapeutic efficacy in preclinical cancer models. However, despite this promise, few of these candidates have been demonstrated to have a meaningful clinical benefit for patients, in part due to tissue-dependent on-target toxicities from the simultaneous repression of both mutant and wild-type NOTCH proteins. The discovery of SERCA as actionable modulators of Notch1 suggested a new targeted approach to treat T-ALL. Uniquely among Notch modulators, SERCA inhibitors preferentially impair the clinically relevant class of oncogenic *NOTCH1* mutants compared to wild type. Thus, the development of tolerated SERCA modulators may uncover a new therapeutic avenue for one of the most frequently mutated genes in human cancers.

In this work, we demonstrated that CAD204520, a novel isoform-specific SERCA inhibitor, exhibits a reduced Ca^{2+} related off-target toxicity but retains anti-Notch1 and anti-leukemia capacity both *in vitro* and *in vivo* in *NOTCH1*-mutated T-ALL models.

To investigate and address potential resistance mechanisms to these SERCA inhibitors, we performed an extensive chemo-transcriptomic analysis on two T-ALL cell lines: one exhibiting resistance and the other sensitivity to TG. The results revealed distinct transcriptomic signatures between the two cell lines. Specifically, we observed an upregulation of steroid metabolism pathways in the resistant cell line. Furthermore, GC showed a higher sensitivity in the TG-resistant cell line compared to the parental one, unveiling a potential role of Notch1-SERCA-GR axis in overcoming GC resistance. Our findings point out SERCA as a regulator of cellular metabolism in T-ALL patients influencing cholesterol synthesis and increasing tumor cell sensitivity to GC.

3. MATERIALS AND METHODS

3.1. Cell Culture

The human cell lines ALL/SIL, MOLT4, DND41, JURKAT, SUPT1 and PF382 were purchased from Leibniz-Institut DSMZ-German collection of microorganisms and cell culture (Germany). The ALL/SIL R cell line was obtained by selecting ALL/SIL cells cultured under gradually increasing concentrations of TG, as previously described. The compound induced missense single-nucleotide polymorphism on *ATP2A2* exon 8 causing Glycine257 to Valine mutation and resistance to TG. Similarly, MOLT4 R cell line was developed by exposing MOLT4 cells to progressively higher concentrations of TG. The TG concentration was increased every two weeks based on the viability of the cells. Cell lines were grown in RPMI 1640 (Thermo Fisher Scientific, Waltham MA, USA) with 10% heat inactivated fetal serum bovine (FBS) (Sigma-Aldrich, St. Louis, MO, USA), 1% penicillin-streptomycin (Thermo Fisher Scientific, Waltham MA, USA) and 2 mM L-Glutamine (Thermo Fisher Scientific, Waltham MA, USA) and incubated at 37°C with 5% CO_2 routinely identified by short tandem repeat profiling, and monitored for mycoplasma contamination.

3.2. Compound library screening

The human T-ALL cell lines ALL/SIL and ALL/SIL R were screened using with the European Chemical Biology Library, provided by EU-OPENSCREEN (Berlin, Germany). A total of 2,464 biologically active compounds were tested at concentrations of 100 nM and 1 µM. The base medium for both cell lines consisted of 90% RPMI 1640, 10% heat inactivated FBS, 1% penicillin-streptomycin and 2 mM L-Glutamine. After 72 hours of incubation, a resazurin fluorescence method was used as a viability assay.

3.3. RNA sequencing

Library preparation Total RNA was extracted from ALL/SIL, and ALL/SIL R. Strand-specific Illumina mRNA libraries were prepared for sequencing, which was performed by Novogene along with, read quality control, alignment (using STAR) to the reference genome (GRCh38) and quantification using HTSeq. Transcript counts were analysed using R (v4.1.2) and they were filtered to retain only transcripts with a coverage of at least 3 in 3 samples. Differential Expression (DE) analysis was performed with DESeq2 by comparing ALL/SIL R to ALL/SIL using default parameters and a BH-adjusted p-value threshold of 0.05 to determine statistically significant DE genes. Gene Set Enrichment Analysis (GSEA) was performed using the ClusterProfiler package with fgsea method and minimum gene set size set to 10 (minGSsize parameter), in total 4 gene sets were used: Ontology gene sets (C5), Kegg (C2), Reactome (C2) and Wikipathways, all downloaded from the molecular signature database (mSigDB). The R package Dorothea provides a list of transcription factor (TF)-target interactions classified based on their confidence level (A-E confidence classes). We selected those interactions having a high confidence level (A, B), and we kept TFs showing 5 or more high-confidence interactions. For each TF, the list of its transcriptional targets was used as a regulon to perform TF activity enrichment analysis with the software viper, which analyses gene expression level of gene targets to infer the activity of upstream regulatory TFs. Viper can be used to estimate TF activity scores at the single-sample level. However, we applied the viper algorithm on a pre-ranked gene list that represented phenotype differences between ALL/SIL R and ALL/SIL cell lines. We used DESeq2 DE results from the comparison between ALL/SIL R and ALL/SIL as input data, and we ordered significant DE genes (adjusted P value < 0.05) based on their DESeq2 stat coefficient (ratio between log2 fold change and fold change standard error). We used the stat (Wald Statistics) coefficient as a gene weight score, then we performed TF activity enrichment analysis on the weighted gene “signature”. Eventually, we obtained a Normalized Enrichment Score

(NES) for each TF regulon activity: a positive NES indicates a higher TF activity in ALL/SIL R, while a negative NES indicates a higher TF activity in ALL/SIL cell line.

We estimated the activity of 14 relevant signaling pathways with the R software PROGENy (Pathway RespOnsive GENes) which uses weighted consensus gene signatures obtained from literature-based perturbation experiments to calculate pathway activity scores. For each pathway, we used the 200 most responsive genes per pathway (based on their weighted score within the pathway consensus signature). In an analogous way to the TF activity analysis described above, we used the ranked list of significant DE genes obtained from DESeq2 analysis, and we used PROGENy to infer a NES for each pathway through a permutation approach. A positive NES indicates a higher pathway activity in ALL/SIL R, while a negative NES indicates a higher pathway activity in ALL/SIL cell line.

3.4. SilR Score

ALL/SIL R similarity (SilR) score for TARGET T-ALL samples was calculated as follows. Briefly, differentially expressed genes (adjusted P value < 0.05, LogFC > 1) between ALL/SIL R and ALL/SIL were filtered to keep only those genes having a minimum level of gene expression variability across samples (log2(FPKM+1) IQR > 1). The selected genes were then divided into up- and down-regulated genes. Genes within each of the two groups were ranked according to the absolute value of their corresponding Wald statistics (higher stat values correspond to lower rank positions). In parallel, log2(FPKM+1) gene expression values of the analyzed samples were ranked following the same strategy, in a sample-wise manner.

For each selected gene in each sample, a score corresponding to the mean between their sample-wise ranking and DE ranking was calculated. Finally, UP and DOWN scores were computed in each sample for up- and down-regulated gene lists, respectively, as the

average of gene-specific scores. Final sample-specific SilR scores correspond to the scaled difference between each UP and DOWN score pair.

3.5. Compound Sources

GC compounds dexamethasone, clobetasol propionate and fluticasone propionate and RU486 were obtined from MedChemExpress EU (MCE) (#HY-14648; #HY-13600; #HY-B0154; #HY-13683). TG was obtained from Enzo Biochem (Enzo Life Science Inc., USA #BML-PE180-0005). CAD204520 was obtained from MedChemExpress EU (MCE) (#HY-164466). The compounds were all dissolved in dimethyl-sulfoxide (DMSO), according to the manufacturer's instructions.

3.6. Cell Treatment and Viability Assay

Cells were then seeded in 384-well plates (Greiner Bio-One, Belgium, #781080) at the final concentration of 0.02 x 10^6 cells/mL per condition using the MultiDrop™ Combi Reagent Dispenser (Thermo Scientific, Waltham, USA, #5840300) peristaltic dispenser. Each compound was added with the nanometric dispenser Tecan D300e (Tecan Trading AG, Switzerland). Cells were incubated in a humidified environment at 37 °C and 5% CO2 for 72 hours. Cell viability was evaluated through the CellTiter-Glo luminescence ATP-based assay (Promega Corporation, Madison, WI, USA, #G7573) and was measured using a Victor X4 Multilabel Plate Reader (Perkin Helmer, Waltham, MA, USA). Output data were then analyzed using GraphPad Prism software version 9 (La Jolla, CA, USA) and a customized R script (RStudio, MA, USA).

3.7. Western Blotting

Protein lysates for western blotting were quantified using the Bio-Rad Protein Assay Dye Reagent (Bio-Rad Laboratories, Hercules, CA, USA, #5000006) and incubated with primary

antibodies specific for the following proteins: cleaved NOTCH1 (Val1744, #4147, Cell Signaling, Beverly, MA, USA), C-terminus of NOTCH1 (XP, #3608, Cell Signaling, Beverly, MA, USA), GR (#3660; Cell Signaling, Beverly, MA, USA) and SERCA2 in ALL/SIL were detected using *ATP2A2* antibody (#9580, Cell Signaling, Beverly, MA, USA). Loading controls were performed with an antibody specific for beta-actin, (#3700, Cell Signaling, Beverly, MA, USA). Blots were developed using species-specific fluorescent antibodies obtained from LI-COR (Biosciences, Lincoln, NE, USA) such as IRDye 680LT Goat anti-Mouse IgG (#925-68020); IRDye 800CW goat anti-rabbit IgG (#925-32211).

3.8. RNA processing and quantification

RNA was extracted using the RNeasy mini kit (Qiagen, Hilden, Germany, #74106). According to the manufacturer's protocol, cDNA was synthesized using the high-capacity cDNA reverse transcription kit (Thermo Fisher Scientific, #4368814), using 1 µg of RNA as starting material. A quantitative real-time polymerase chain reaction (qPCR) was performed using TaqMan gene expression assays for NR3C1 (Thermo Fisher Scientific, #Hs00353740_m1), and TaqMan™ Universal PCR master mix (Thermo Fisher Scientific, #4364338) in an Applied Biosystems™ StepOne™ real-time PCR system (Thermo Fisher Scientific, #4376357). Each condition was run in triplicate. The expression levels of the target genes were normalized to those of RPL13A (Thermo Fisher Scientific, #Hs04194366_g1). Data were analyzed using the ΔΔ cycle threshold (CT) method and plotted as a percentage relative to control.

3.9. Immunohistochemistry

Hematoxylin and eosin (H&E), periodic acid-Schiff (PAS), and immunohistochemical (IHC) stainings were performed on 4µm serial sections of formalin-fixed paraffin-embedded (FFPE) of mice spleen, kidney, liver, bowel, and bone marrow tissues. Primary antibodies

employed in immunoperoxidase staining were mouse anti-human CD45 (DAKO; M0701; 1:100; room temperature; 30 minutes). All sections were revealed by the IHC Detection Kit-Micropolymer (Abcam; ab236466) according to manufacturer's recommendations. Hematoxylin was used as the counterstain and closed with coverslips. The evaluation of immunostaining was performed using light microscope (Olympus BX60) connected with a digital camera (QICAM) and quantified using QuPath software v.0.3.2 (https://qupath.github.io/).

3.10. *In vivo* studies

NOD-*SCID* IL2Rgamma^{null} (NSG) mice (The Jackson labs, RRID: IMSR_JAX:005557) for efficacy studies were maintained in specific pathogen-free facilities at the University of Parma (Department of Food and Drug Science, Cod. BDNS. 4CEB4 Via: Parco Area delle Scienze 27/A Parma - PR). Animals were housed in a temperature-controlled room (22–24°C), with a 12-hour light cycle (light on from 7.00 AM to 7.00 PM) with unrestricted food and water supply. Animal procedures were approved by the University of Parma (Protocol N.682/2019-PR) guidelines for the protection of animals used for scientific purposes.

For each PDX sample, 10x10^6 cells in 200 µL of phosphate buffer saline (PBS) were injected in tail vein in adult (6 weeks old) non-irradiated NSG mice. Leukemic cell engraftment was monitored every 7 days by flow cytometry of peripheral blood cells stained with an anti-human CD45-PE antibody (BD Bioscience, Franklyn Lakes, NJ, USA, #560975, HI30 clone). For efficacy studies, T-ALL leukemia cells (10 x 10^6) from the PDLX were transplanted by tail vein injection in 6 weeks old male. Engraftment of human PDLX cells was monitored every 4 days by flow cytometry of peripheral blood stained with an anti-human CD45-PE antibody. Eight mice per condition received the treatment upon engraftment, defined as ≥0.5% peripheral blood human CD45+/human cells. Mice received CAD204520 in the fed state by oral gavage dissolved in Tween-80 0.5% (Sigma-Aldrich, Missouri, USA) and

hydroxypropyl-methylcellulose (HPMC) 1.0% (Sigma-Aldrich, Missouri, USA) at a dose of 30 mg/kg bid day 1-5, day 8-12, and day 15-19. Dexamethasone by intraperitoneal injection at a dose of 5 mg/kg/die day 1-3-5, day 8-10-12, and day 15-17-19: both or control vehicle by oral gavage (Tween 80 0.5%, w/v, and hydroxypropyl-methylcellulose [HPMC] 1.0%), respectively. The antileukemic activity of drug combination in mice was assessed by a survival study (Kaplan-Meier method), and by measuring hCD45 expression on bone marrow and peripheral blood by flow cytometry (Attune NxT Flow Cytometer, Thermo Fisher Scientific, Waltham MA, USA).

3.11. Statistical analysis

Statistical analyses were performed using GraphPad Prism 8 or R software. The assumption of normal distribution was not determined, and the P value among samples was calculated by a non-parametric t-test (Mann-Whitney) by comparing treated samples to untreated controls. We used one- or two-way ANOVA using statistical correction for multiple comparison algorithms, as specified in the figure legends, to determine appropriate significance among groups. Statistical significance, group size, and experimental details are described in the figure legends.

4. RESULTS

4.1. Characterization of SERCA Inhibitor Binding: CAD204520 and TG

SERCA can be suppressed by various small molecules, such as TG, BHQ, 1,3-dibromo-2,4,6-tris(methyl-isothio-uronium) benzene, and CPA. These compounds target distinct binding sites on the ATPase protein, resulting in unique modes of inhibition (71). An important question is whether CAD204520's binding to SERCA replicates the ATPase inhibition kinetics seen with TG or if, as suggested by structural data, the two molecules function independently (**Figure 1A**). To test our hypothesis, we generated a T-ALL cell line (ALL/SIL) resistant to TG by selecting cells growing under increasing concentrations of this molecule (55). To investigate potential TG-induced mutations within the SERCA encoding genes, *ATP2A1–3*, we conducted whole-exome sequencing focusing our analysis specifically on exonic single-nucleotide missense variants. Interestingly, in ALL/SIL resistant cells (ALL/SIL R) we identified, within the Asp254-Leu260 hotspot, a missense single-nucleotide polymorphism occurring in *ATP2A2* exon 8 (c.G770T) causing a Glycine257/Valine mutation in the M3 helix (**Figure 1B**). No mutations occurred in *ATP2A1* (**Figure 1C**), while missense mutations in *ATP2A3* were present both in the parental and resistant lines, indicating a pre-existing mechanism of allelic variance. Next, we treated ALL/SIL parental and resistant cells at ALL/SIL IC50 concentrations and demonstrated that p.G257V rescues ALL/SIL cells from TG-induced cytotoxicity while it does not interfere with CAD204520 effects (**Figure 1D**).

Accordingly, because CAD204520 binds to SERCA in a pocket similar to that of CPA but distinct to that of TG, we anticipated that the combined inhibition might result in a synergistic effect with TG but not with CPA. To avoid the limitations and biases associated with any one algorithm used to study drug interactions, we used comprehensive approaches, including the Loewe additivity model, the Chou and Talalay index. The Loewe additivity is a commonly

used dose-effect-based model to quantify a zero-interactive state for the combination of two drugs (72). The Chou-Talalay method (73) for drug combination is based on the median-effect equation and provides a mechanism-independent method for quantitative determination, combination index (CI), of drug interactions. A CI ranging from 0.9 to 1.1 is considered additive, a CI < 0.9 indicates synergy, and a CI > 1.1 resistance. We tested CAD204520 and TG in combination at the indicated concentrations for a total of 60 combinatorial points in T-ALL cell lines. We found that simultaneous exposure to CAD204520 and TG for 72 h resulted in a robust synergistic inhibition of cell viability in T-ALL cells (**Figure 1E-F**).

Together, these data show that CAD204520 selectively binds SERCA in the same binding pocket as BHQ, CPA and that that p.G257V mutation in the M3 helix of SERCA do not interfere with CAD204520 activity and that a greater anti-leukemia effect may be achieved by the simultaneous binding of CAD204520 and TG to their respective sites in SERCA.

4.2. Transcriptomic analysis reveals an upregulation of steroids metabolism

To identify relevant pathways that may be dysregulated by *ATP2A2* mutation, we performed an RNA sequencing (RNAseq) analysis in ALL/SIL and ALL/SIL R cell lines. Interestingly, despite a similar growth rate, parental and resistant cells showed 6241 differentially expressed (DE) genes (**Figure 2A-B**). We next performed gene set analysis on our transcriptional data, identifying an enrichment of pathways associated with steroid metabolism, including cholesterol biosynthesis and metabolism, lipid biosynthesis and metabolism, and response to sterol (**Figure 2C**).

In parallel, we performed a transcription factor (TF) enrichment analysis on the upregulated gene set (**Figure 2D**). This analysis identified transcription factors likely to play significant roles in regulating the expression of these genes. Sterol Regulatory Element-Binding Protein 1 and 2 (SREBP1-2) were enriched among the transcription factors associated with the

upregulated genes. SREBP1 is a key regulator of lipid biosynthesis, particularly influencing genes involved in fatty acid and cholesterol metabolism, consistent with the functional pathways enriched in our dataset (74).

Piovan et al. highlighted that the activation of one or more oncogenic signaling pathways involved in T-cell transformation may drive primary GC resistance in T-ALL either by directly disrupting GR functionality or indirectly by suppressing GC-induced apoptosis (23,67). In this framework, the PI3K-AKT-mTOR signaling cascade plays a major role in the pathogenesis of T-ALL, particularly in leukemias harboring mutations and deletions in the *PTEN* tumor suppressor gene. In line with these findings, our pathway enrichment analysis revealed the involvement of PI3K pathway in the ALL/SIL R transcriptomic signature, supporting the investigation GC activity as a potential novel mechanism for anticipating resistance to SERCA inhibition (**Figure 2E**).

4.3. TG resistance exhibits a sensitivity profile to GCs activity in *NOTCH1*-mutated cell line carrying *ATP2A2* mutation

To anticipate the potential mechanism of resistance to SERCA inhibitors and identify synthetic lethality in the TG-resistant T-ALL cell line, we performed a small molecule screening with nearly 2,464 bioactive compounds from the European Chemical Biology Library provided by EU-OPENSCREEN. The compounds were tested with 1 µM and 100 nM concentrations. Compound hits were flagged based on their ability to preferentially inhibit either ALL/SIL or ALL/SIL R cell lines, or both. The two cell lines displayed a different sensitivity profile, with 105 compounds that showed the same activity in both models (**Figure 3A**). Only three compounds—birinapant (an IAP inhibitor), GSK461364 (a PLK inhibitor), and zotarolimus (a rapamycin analog targeting the FKBP12-binding protein upstream of mTOR)—were specifically active in parental ALL/SIL cells compared to the resistant cell line (**Figure 3B**). We observed greater sensitivity in ALL/SIL R cells compared to the parental

cell line, with 163 compounds displaying a specific cytotoxic effect in the ALL/SIL R cells at 100 nM concentration (**Figure 3C**). RNA-Seq analysis highlighted the involvement of steroid metabolism, prompting us to evaluate the response of the two cell lines (ALL/SIL and ALL/SIL R) to steroid-based drugs, particularly drugs, specifically those that modulate nuclear receptor activity, such as glucocorticoids and other steroid hormone analogs. Among these, only GC treatment resulted in higher activity in the TG-resistant cell line than the parental one. No differences between the two models were identified for other steroid-based small molecules targeting androgen, estrogen, mineralocorticoid, and progesterone receptors (**Figure 3D**). Surprisingly with the sequencing data, we identified GCs as compounds with preferential activity in ALL/SIL R cell line and were used for further validations.

4.4. The *ATP2A2* mutation induces upregulation and functional restoration of the GR in ALL/SIL R cells.

To determine whether the increased sensitivity to GCs was associated with upregulation of the specific nuclear receptor, we performed immunoblotting for GR in six human T-ALL cell lines (ALL/SIL, ALL/SIL R, DND41, JURKAT, PF382, SUPT1). We confirmed a significant increase in GR levels in ALL/SIL R compared to the other cell lines despite no differences being identifiable in the Notch1 pathway subunit protein levels (**Figure 4A**).To test if the function of SERCA and its sensitivity to SIs consistently induced a rescue of GC resistance in T-ALL, we generated additional T-ALL cell lines models (MOLT4) with resistance (R) to TG using the same stepwise TG increased concentration treatment. The immunoblotting confirmed GR upregulation also in MOLT4 R. Real-time quantitative PCR (RT-PCR) confirmed the overexpression of GR in ALL/SIL R and MOLT4 R relative to the parental cell line (**Figure 4B**).

In addition, we validated the higher sensitivity at low nanomolar concentrations of the ALL/SIL R to three different GCs (dexamethasone, clobetasol propionato, and fluticasone propionato) compared to the parental cell lines and other T-ALL, as expected (**Figure 4C**).

To determine whether GC sensitivity was mediated by a soluble factor induced by SERCA mutation, we incubated different T-ALL cell lines with conditioned media from ALL/SIL R cells and then treated them with GCs. However, the ALL/SIL R-conditioned media did not restore corticosteroid sensitivity in the parental line or the other T-ALL cell lines (**Figure 4D**). This finding confirmed that the modification of the GC sensitivity is related to an intrinsic transcriptomic profile reprogramming of the resistant cell line.

Finally, to test the dependency of the GC sensitivity to the GR upregulation, we used a well-known specific GR inhibitor, RU-486 for a competition assay, as follows. The parental and resistant cell lines were treated with three different GCs (dexamethasone, clobetasol, and fluticasone) as a single treatment, in combination with the ALL/SIL IC50 concentration of TG (10 nM), and in combination with TG IC50 and 1 μM RU-486. As expected, the three GC alone were only active in the resistant cell line compared to the parental one. When 10 nM TG was added to the assay, in line with the high grade of resistance, no modification to the GC dose-response curve in the ALL/SIL R was detectable. In parallel, the ALL/SIL dose-response curve in the presence of the stable IC50 10 nM concentration of TG showed a constant plateau on 50% of cells inhibited. Finally, pretreatment with RU-486 reduced the sensitivity of ALL/SIL R cells to the GC-TG combination (**Figure 4E**). These data confirmed that the *ATP2A2* mutation drives a metabolic adaptation characterized by upregulation of GR and restored sensitivity to GC treatment.

4.5. SERCA inhibitors exhibit synergy with GCs

Previous studies have demonstrated that GSI can reverse GC resistance, supporting the potential of combinatorial therapy in GC-resistant T-ALL (45,75). To evaluate whether GCs

can synergize with SERCA inhibitors independently of *ATP2A2* mutation status, overcoming resistance to SERCA inhibition, we treated both sensitive and resistant cell lines with a combination of a SERCA inhibitor (TG or CAD204520) and a GC (dexamethasone, clobetasol propionate, or fluticasone propionate) for 72 hours (**Figure 4F**).To analyze synergy, we used the Loewe model and the Chou-Talalay combination index approaches, as previously described.

The association of SERCA inhibitors plus steroids displayed a synergistic effect at low dose combination in both cell lines, with a more pronounced ALL/SIL R activity that harbors the *ATP2A2* mutation, highlighting a promising combination effect for translation application of this treatment (**Figure 4F-G**).

4.6. The SERCA mutant cell line clusters with TAL/LMO genetic subgroup

ATP2A2 mutation is not typically included in routine diagnostic evaluations, making the identification of GC-sensitive cases difficult to identify. For this reason, we developed a transcriptomic score based on the down and up-regulated gene signature of the ALL/SIL R and ALL/SIL (silR score). We compared the signature to available transcriptional data from publicly available T-ALL datasets. Samples with high silR score were identified as showing a gene expression profile more similar to the one of ALL/SIL R. On the contrary samples with low silR score were identified as showing a gene expression profile more similar to the one of the parentals ALL/SIL cell line. Analysis of two independent pediatric and adult T-ALL datasets (15,76) showed that samples with a high SilR score predominantly belong to the *TAL1/LMO* genetic subgroup (**Figure 5A-B**).

As part of our translational strategy, we aimed to test the effects of CAD204520 and dexamethasone in primary T-ALL samples belonging to the TAL/LMO subgroup collected in our laboratory (**Figure 5C**). Samples with TAL1 rearrangement showed a favorable response to the combination of CAD204520 and dexamethasone, compared to

monotherapy (**Figure 5B and 5C**), confirming our hypothesis. These samples were subsequently used for *in vivo* validation.

4.7. The combination of GC and CAD204520 displays an anti-leukemia activity in a TAL1-rearranged T-ALL Model *in vivo*

To validate the efficacy of the combination between CAD204520 and dexamethasone *in vivo*, we established a patient-derived leukemia xenograft (PDLX) model using a primary T-ALL sample with *NOTCH1* mutation and *TAL1* rearrangement. Following disease establishment, the mice were treated for 21 days with vehicle or CAD204520 at a dose of 30 mg/kg BID on days 1-5, 8-12, and 15-19 with a washout period on days 6-7 and 13-14. Dexamethasone was administered at 5 mg/kg/die on days 1-3-5, 8-10-12, and 15-17-19 (**Figure 6A**) with washout on the same days. The combination therapy effectively inhibited the progression of leukemic cells in both peripheral blood and bone marrow of treated mice compared to vehicle-treated control, as evidenced by the tracking of hCD45+. (**Figure 6B and 6C**). Additionally, the treatment led to a consistent reduction in leukemic infiltration within the spleen (**Figure 6D**). Moreover, mice treated with the combination showed a mild reduction of weight (**Figure 6E**) without general signs of toxicity. Next, an assessment of the combination therapy 's effect on the bone marrow was conducted via immunohistochemistry (HIC), revealing a nearly complete loss of CD45+ leukemic cells in treated animals compared to those treated with the vehicle control (**Figure 6F**). CD45 expression mirrored the extent of tumor infiltration (**Figure 6G**).

These data highlight the efficacy of the GC-SERCA combination in a specific T-ALL subgroup, paving the way for a more specific and comprehensive characterization of steroid resistance and rescue and correlation with the Notch1-SERCA axis.

5. DISCUSSION

T-cell acute lymphoblastic leukemia is a highly proliferative hematologic malignancy that results from a multistep transformation process where accumulating genetic alterations disrupt key oncogenic, tumour suppressor and developmental pathways responsible for the normal control of cell growth, proliferation, survival and differentiation during thymocyte development. The high prevalence of *NOTCH1*-activating mutations (60%) in T-ALL provides a strong rationale for the development of targeted strategies toward inhibition of Notch signaling. However, pan Notch pathway antagonists such as GSI, while reduce leukemia growth in mutant cancer cell lines and in mouse models, might cause prolonged suppression of the canonical Notch pathway in normal tissue with subsequent dose limiting gastrointestinal toxicity (77) or increase the risk of skin cancers (78). Appropriate NOTCH subcellular localization is crucial and provides the time and space context for its activation. The succession of “S” cleavages is tightly regulated and, consequently, the subcellular mislocalization of NOTCH proteins might represent an attractive strategy for therapeutic interventions. We and others have been pioneers in the research of this strategy, identifying SERCA as a liable regulator of Notch signaling. Indeed, SERCA inhibition is considered a potential strategy to block consequently the activity of mutated *NOTCH1* gene without any off-target effect on the wild type of pathway (79).

Because of the low tolerability of TG in terms of cardiac toxicity due to its off-target effect and disruption of homeostasis of Ca^{2+}, limiting its activity in the clinical setting. To overcome this limitation, Marchesini and colleagues optimized a novel SERCA inhibitor, CAD204520, that displayed a different binding site on the SERCA pump compared to the one of TG, and retained the same anti-leukemia and anti-NOTCH1 properties without the main off-target toxicity on cardiac tissue (55).

In our study, we began with a human T-ALL cell line previously made resistant to TG. This resistance was attributed to a missense mutation on *ATP2A2* exon 8, resulting in a Glycine257 to Valine mutation. Our objective was to explore ways to anticipate resistance to SERCA inhibitors. Although ALL/SIL R are resistant to TG, they remained sensitive to CAD204520 due to the different binding site to SERCA. To dissect the different sensitivity of the two related cell lines, we coupled a transcriptomic screening and small molecule screening. From a gene expression point of view, the two models clearly showed different transcriptional programs of the cell metabolic behavior, characterized by significant upregulation of metabolic pathways related to cholesterol synthesis, response to sterol and more in general to the metabolism of steroids. This result suggested that the simple hotspot mutation that alters the function of SERCA may induce a strong modification of the steroid and cholesterol signaling pathway, hypothesizing a close relationship between Ca^{2+} homeostasis and lipid metabolism. Some studies have already attempted to identify a connection between Ca^{2+}-ATPases and cholesterol (80) but the result was not confirmed by other authors (81). In parallel, we performed a small molecules screening with nearly 2500 bioactive compounds from the ECBL. Consistent with the differential behavior observed in the transcriptomic analysis, we confirmed distinct sensitivities between the ALL/SIL and ALL/SIL R cell lines. Specifically, based on the upregulation of lipid metabolism and the response to sterols identified in the Gene Set Enrichment Analysis (GSEA), we focused our investigation on nuclear receptor inhibitors. Notably, we found that GCs exhibited specific activity against the resistant cell line. As evidence of GC resistance reversal, we observed an upregulation of the PI3K pathway, reflected by an increased NES, consistent with findings from other studies (67). We then investigated whether the restored sensitivity to GCs was linked to the GR. As expected, GR expression was elevated at both the gene and protein levels in the ALL/SIL R cell line compared to the parental line and a panel of other T-ALL cell lines. Correspondingly, TG-resistant cells showed heightened sensitivity to various GCs,

including dexamethasone, clobetasol, and fluticasone, in a dose-dependent manner. Generally, T-ALL patients showing increasing resistance to GC therapy may be related to the inability of leukemic cells to up-regulate the GR upon GC exposure, identifying GC resistance as a major contributor to treatment failure [74]. A study by Real et al. proposed that upregulation of GR expression in response to GCs could reduce resistance in ALL (45). In our study, we demonstrated that GR upregulation in the resistant cell line was responsible for the increased sensitivity to GCs. Specifically, treatment with the GR antagonist RU486 reduced GC efficacy in ALL/SIL R confirming R dependency in the *ATP2A2*-mutated cell line. This suggests that the *SERCA* gene mutation may trigger a metabolic shift, leading to GR upregulation and heightened GC sensitivity. To further validate this hypothesis, we induced TG resistance in another *NOTCH1*-mutated T-ALL cell line, MOLT4. After obtaining the resistant MOLT4 cells (MOLT4 R), we confirmed GR upregulation via immunoblotting. Like ALL/SIL R, these cells showed increased GC sensitivity while maintaining resistance to TG but retaining sensitivity to CAD treatment.

Building on previous findings by Real et al. showing synergistic activity between GSIs and GCs in reversing GC resistance in T-ALL (45), we investigated the potential synergy between the SERCA inhibitor CAD204520 and GCs. The combination demonstrated a synergistic effect at low doses in both cell lines, with greater efficacy in ALL/SIL R harboring the *ATP2A2* mutation, highlighting a promising therapeutic strategy for T-ALL patients.

To facilitate clinical translation, we developed a SilR score based on the ALL/SIL R gene expression profile. Patients with transcriptional profiles resembling the TAL1 subgroup were predominantly classified in the high SilR score group, highlighting the similarity between these contexts. Consistently, TAL1 subgroup patients with *NOTCH1* mutations and resistance to SERCA inhibitors exhibited increased sensitivity to dexamethasone and a strong synergistic response to combined CAD204520 and dexamethasone treatment.

Finally, to validate our in vitro findings, we used a T-ALL patient-derived xenograft (PDX) model established from primary blasts of a TAL1 case with a high SilR score, mirroring the characteristics of ALL/SIL R. In vivo, the combination of CAD204520 and dexamethasone demonstrated significant anti-leukemic activity without inducing toxicity or weight loss. These results highlight the potential clinical relevance of combining SERCA inhibitors with GCs as an effective strategy for T-ALL, particularly in patients resistant to conventional therapies. Further preclinical and clinical studies are needed to confirm these findings and assess their translational potential.

6. CONCLUSIONS

In conclusion, our study aimed to address the challenge of anticipating resistance to SERCA inhibitors in *NOTCH1*-mutated T-ALL. Our findings revealed that prolonged exposure to TG led to mutations in the *ATP2A2* gene at the ligand binding site. Interestingly, this mutation exerted selective pressure on the malignant clone, resulting in a transcriptional profile more strongly associated with the TAL1 subgroup and increased sensitivity to GCs. Furthermore, our *in vivo* experiments showed that the combination of SERCA inhibitors and GCs exhibited enhanced anti-leukemic activity without causing toxicity or weight loss. These findings highlight the potential for this combination strategy to be translated into a targeted clinical approach for treating *NOTCH1*-mutated T-ALL. By combining SERCA inhibitors with steroids, we not only improve therapeutic efficacy but also provide a more targeted strategy that minimizes toxicity compared to conventional treatments, thereby improving the safety and tolerability of treatment regimens for patients affected by this disease.

7. BIBLIOGRAPHY

1. Brown PA, Shah B, Fathi A, Wieduwilt M, Advani A, Aoun P, et al. NCCN Guidelines Insights: Acute Lymphoblastic Leukemia, Version 1.2017. J Natl Compr Canc Netw. settembre 2017;15(9):1091–102.

2. Follini E, Marchesini M, Roti G. Strategies to Overcome Resistance Mechanisms in T-Cell Acute Lymphoblastic Leukemia. Int J Mol Sci. 20 giugno 2019;20(12):3021.

3. Weng AP, Ferrando AA, Lee W, Morris JP, Silverman LB, Sanchez-Irizarry C, et al. Activating Mutations of NOTCH1 in Human T Cell Acute Lymphoblastic Leukemia. Science. 8 ottobre 2004;306(5694):269–71.

4. Sanchez-Martin M, Ferrando A. The NOTCH1-MYC highway toward T-cell acute lymphoblastic leukemia. Blood. 2 marzo 2017;129(9):1124–33.

5. Van der Meulen J, Van Roy N, Van Vlierberghe P, Speleman F. The epigenetic landscape of T-cell acute lymphoblastic leukemia. Int J Biochem Cell Biol. agosto 2014;53:547–57.

6. Rothenberg EV. Epigenetic mechanisms and developmental choice hierarchies in T-lymphocyte development. Briefings in Functional Genomics. 6 agosto 2013;12(6):512.

7. Durinck K, Goossens S, Peirs S, Wallaert A, Van Loocke W, Matthijssens F, et al. Novel biological insights in T-cell acute lymphoblastic leukemia. Exp Hematol. agosto 2015;43(8):625–39.

8. Puckett Y, Chan O. Acute Lymphocytic Leukemia. In: StatPearls [Internet]. Treasure Island (FL): StatPearls Publishing; 2024 [citato 12 novembre 2024]. Disponibile su: http://www.ncbi.nlm.nih.gov/books/NBK459149/

9. Neumann M, Beder T, Bastian L, Hänzelmann S, Bultmann M, Wolgast N, et al. Molecular subgroups of T-cell acute lymphoblastic leukemia in adults treated according to pediatric-based GMALL protocols. Leukemia. giugno 2024;38(6):1213–22.

10. Parkin DM, Stiller CA, Draper GJ, Bieber CA. The international incidence of childhood cancer. Int J Cancer. 15 ottobre 1988;42(4):511–20.

11. Bardelli V, Arniani S, Pierini V, Giacomo DD, Pierini T, Gorello P, et al. T-Cell Acute Lymphoblastic Leukemia: Biomarkers and Their Clinical Usefulness. Genes. 23 luglio 2021;12(8):1118.

12. Goldberg JM, Silverman LB, Levy DE, Dalton VK, Gelber RD, Lehmann L, et al. Childhood T-cell acute lymphoblastic leukemia: the Dana-Farber Cancer Institute acute lymphoblastic leukemia consortium experience. J Clin Oncol. 1 ottobre 2003;21(19):3616–22.

13. Chiaretti S, Zini G, Bassan R. Diagnosis and subclassification of acute lymphoblastic leukemia. Mediterr J Hematol Infect Dis. 2014;6(1):e2014073.

14. Sin CF, Man PHM. Early T-Cell Precursor Acute Lymphoblastic Leukemia: Diagnosis, Updates in Molecular Pathogenesis, Management, and Novel Therapies. Front Oncol. 2021;11:750789.

15. Liu Y, Easton J, Shao Y, Maciaszek J, Wang Z, Wilkinson MR, et al. The genomic landscape of pediatric and young adult T-lineage acute lymphoblastic leukemia. Nat Genet. agosto 2017;49(8):1211–8.

16. Soulier J, Clappier E, Cayuela JM, Regnault A, García-Peydró M, Dombret H, et al. HOXA genes are included in genetic and biologic networks defining human acute T-cell leukemia (T-ALL). Blood. 1 luglio 2005;106(1):274–86.

17. Xia Y, Brown L, Yang CY, Tsan JT, Siciliano MJ, Espinosa R, et al. TAL2, a helix-loop-helix gene activated by the (7;9)(q34;q32) translocation in human T-cell leukemia. Proc Natl Acad Sci U S A. 15 dicembre 1991;88(24):11416–20.

18. Royer-Pokora B, Loos U, Ludwig WD. TTG-2, a new gene encoding a cysteine-rich protein with the LIM motif, is overexpressed in acute T-cell leukaemia with the t(11;14)(p13;q11). Oncogene. ottobre 1991;6(10):1887–93.

19. The genetics and molecular biology of T-ALL | Blood | American Society of Hematology [Internet]. [citato 20 marzo 2023]. Disponibile su: https://ashpublications.org/blood/article/129/9/1113/36559/The-genetics-and-molecular-biology-of-T-ALL

20. Van Vlierberghe P, Ambesi-Impiombato A, De Keersmaecker K, Hadler M, Paietta E, Tallman MS, et al. Prognostic relevance of integrated genetic profiling in adult T-cell acute lymphoblastic leukemia. Blood. 4 luglio 2013;122(1):74–82.

21. Zhang J, Ding L, Holmfeldt L, Wu G, Heatley SL, Payne-Turner D, et al. The genetic basis of early T-cell precursor acute lymphoblastic leukaemia. Nature. 11 gennaio 2012;481(7380):157–63.

22. Ntziachristos P, Tsirigos A, Van Vlierberghe P, Nedjic J, Trimarchi T, Flaherty MS, et al. Genetic inactivation of the polycomb repressive complex 2 in T cell acute lymphoblastic leukemia. Nat Med. 6 febbraio 2012;18(2):298–301.

23. Palomero T, Sulis ML, Cortina M, Real PJ, Barnes K, Ciofani M, et al. Mutational loss of PTEN induces resistance to NOTCH1 inhibition in T-cell leukemia. Nat Med. ottobre 2007;13(10):1203–10.

24. Mendes RD, Sarmento LM, Canté-Barrett K, Zuurbier L, Buijs-Gladdines JGCAM, Póvoa V, et al. PTEN microdeletions in T-cell acute lymphoblastic leukemia are caused by illegitimate RAG-mediated recombination events. Blood. 24 luglio 2014;124(4):567–78.

25. Shochat C, Tal N, Bandapalli OR, Palmi C, Ganmore I, te Kronnie G, et al. Gain-of-function mutations in interleukin-7 receptor-α (IL7R) in childhood acute lymphoblastic leukemias. J Exp Med. 9 maggio 2011;208(5):901–8.

26. Zenatti PP, Ribeiro D, Li W, Zuurbier L, Silva MC, Paganin M, et al. Oncogenic IL7R gain-of-function mutations in childhood T-cell acute lymphoblastic leukemia. Nat Genet. 4 settembre 2011;43(10):932–9.

27. Malecki MJ, Sanchez-Irizarry C, Mitchell JL, Histen G, Xu ML, Aster JC, et al. Leukemia-associated mutations within the NOTCH1 heterodimerization domain fall into at least two distinct mechanistic classes. Mol Cell Biol. giugno 2006;26(12):4642–51.

28. Structure and Function of the γ-Secretase Complex - PMC [Internet]. [citato 20 febbraio 2023]. Disponibile su: https://www.ncbi.nlm.nih.gov/pmc/articles/PMC6618299/

29. Pagliaro L, Chen SJ, Herranz D, Mecucci C, Harrison CJ, Mullighan CG, et al. Acute lymphoblastic leukaemia. Nat Rev Dis Primers. 13 giugno 2024;10(1):1–28.

30. Kopan R, Ilagan MXG. The canonical Notch signaling pathway: unfolding the activation mechanism. Cell. 17 aprile 2009;137(2):216–33.

31. Seegar TCM, Killingsworth LB, Saha N, Meyer PA, Patra D, Zimmerman B, et al. Structural Basis for Regulated Proteolysis by the α-Secretase ADAM10. Cell. 14 dicembre 2017;171(7):1638-1648.e7.

32. Du H, Shih CH, Wosczyna MN, Mueller AA, Cho J, Aggarwal A, et al. Macrophage-released ADAMTS1 promotes muscle stem cell activation. Nat Commun. 22 settembre 2017;8(1):669.

33. Li YM, Lai MT, Xu M, Huang Q, DiMuzio-Mower J, Sardana MK, et al. Presenilin 1 is linked with gamma-secretase activity in the detergent solubilized state. Proc Natl Acad Sci U S A. 23 maggio 2000;97(11):6138–43.

34. Li YM, Xu M, Lai MT, Huang Q, Castro JL, DiMuzio-Mower J, et al. Photoactivated γ-secretase inhibitors directed to the active site covalently label presenilin 1. Nature. giugno 2000;405(6787):689–94.

35. Kimberly WT, LaVoie MJ, Ostaszewski BL, Ye W, Wolfe MS, Selkoe DJ. Gamma-secretase is a membrane protein complex comprised of presenilin, nicastrin, Aph-1, and Pen-2. Proc Natl Acad Sci U S A. 27 maggio 2003;100(11):6382–7.

36. Huenniger K, Krämer A, Soom M, Chang I, Köhler M, Depping R, et al. Notch1 signaling is mediated by importins alpha 3, 4, and 7. Cellular and Molecular Life Sciences: CMLS. 8 maggio 2010;67(18):3187.

37. Pagliaro L, Sorrentino C, Roti G. Targeting Notch Trafficking and Processing in Cancers. Cells. 29 settembre 2020;9(10):2212.

38. Girardi T, Vicente C, Cools J, De Keersmaecker K. The genetics and molecular biology of T-ALL. Blood. 2 marzo 2017;129(9):1113–23.

39. Palomero T, Barnes KC, Real PJ, Glade Bender JL, Sulis ML, Murty VV, et al. CUTLL1, a novel human T-cell lymphoma cell line with t(7;9) rearrangement, aberrant

NOTCH1 activation and high sensitivity to gamma-secretase inhibitors. Leukemia. luglio 2006;20(7):1279–87.

40. Weng AP, Ferrando AA, Lee W, Morris JP, Silverman LB, Sanchez-Irizarry C, et al. Activating mutations of NOTCH1 in human T cell acute lymphoblastic leukemia. Science. 8 ottobre 2004;306(5694):269–71.

41. Toyoshima C, Sasabe H, Stokes DL. Three-dimensional cryo-electron microscopy of the calcium ion pump in the sarcoplasmic reticulum membrane. Nature. 1 aprile 1993;362(6419):467–71.

42. Zhang P, Toyoshima C, Yonekura K, Green NM, Stokes DL. Structure of the calcium pump from sarcoplasmic reticulum at 8-A resolution. Nature. 23 aprile 1998;392(6678):835–9.

43. Marchesini M, Gherli A, Montanaro A, Patrizi L, Sorrentino C, Pagliaro L, et al. Blockade of Oncogenic NOTCH1 with the SERCA Inhibitor CAD204520 in T Cell Acute Lymphoblastic Leukemia. Cell Chem Biol. 18 giugno 2020;27(6):678-697.e13.

44. Pagliaro L, Marchesini M, Roti G. Targeting oncogenic Notch signaling with SERCA inhibitors. J Hematol Oncol. 6 gennaio 2021;14(1):8.

45. Real PJ, Tosello V, Palomero T, Castillo M, Hernando E, de Stanchina E, et al. Gamma-secretase inhibitors reverse glucocorticoid resistance in T cell acute lymphoblastic leukemia. Nat Med. gennaio 2009;15(1):50–8.

46. Olesen C, Picard M, Winther AML, Gyrup C, Morth JP, Oxvig C, et al. The structural basis of calcium transport by the calcium pump. Nature. 13 dicembre 2007;450(7172):1036–42.

47. Roti G, Stegmaier K. New Approaches to Target T-ALL. Front Oncol. 2014;4:170.

48. Lipskaia L, Hulot JS, Lompré AM. Role of sarco/endoplasmic reticulum calcium content and calcium ATPase activity in the control of cell growth and proliferation. Pflugers Arch. gennaio 2009;457(3):673–85.

49. Periz G, Fortini ME. Ca(2+)-ATPase function is required for intracellular trafficking of the Notch receptor in Drosophila. EMBO J. 1 novembre 1999;18(21):5983–93.

50. Ball M, Andrews SP, Wierschem F, Cleator E, Smith MD, Ley SV. Total synthesis of thapsigargin, a potent SERCA pump inhibitor. Org Lett. 15 febbraio 2007;9(4):663–6.

51. Denmeade SR, Mhaka AM, Rosen DM, Brennen WN, Dalrymple S, Dach I, et al. Engineering a prostate-specific membrane antigen-activated tumor endothelial cell prodrug for cancer therapy. Sci Transl Med. 27 giugno 2012;4(140):140ra86.

52. C DF, B H, F H, R M, T F, C B, et al. The clerodane diterpene casearin J induces apoptosis of T-ALL cells through SERCA inhibition, oxidative stress, and interference with

Notch1 signaling. Cell death & disease [Internet]. 28 gennaio 2016 [citato 25 marzo 2023];7(1). Disponibile su: https://pubmed.ncbi.nlm.nih.gov/26821066/

53. De Ford C, Heidersdorf B, Haun F, Murillo R, Friedrich T, Borner C, et al. The clerodane diterpene casearin J induces apoptosis of T-ALL cells through SERCA inhibition, oxidative stress, and interference with Notch1 signaling. Cell Death Dis. 28 gennaio 2016;7(1):e2070.

54. Cialfi S, Palermo R, Manca S, Checquolo S, Bellavia D, Pelullo M, et al. Glucocorticoid sensitivity of T-cell lymphoblastic leukemia/lymphoma is associated with glucocorticoid receptor-mediated inhibition of Notch1 expression. Leukemia. febbraio 2013;27(2):485–8.

55. Marchesini M, Gherli A, Montanaro A, Patrizi L, Sorrentino C, Pagliaro L, et al. Blockade of Oncogenic NOTCH1 with the SERCA Inhibitor CAD204520 in T-cell Acute Lymphoblastic Leukemia. Cell Chem Biol. 18 giugno 2020;27(6):678-697.e13.

56. Olivas-Aguirre M, Torres-López L, Pottosin I, Dobrovinskaya O. Overcoming Glucocorticoid Resistance in Acute Lymphoblastic Leukemia: Repurposed Drugs Can Improve the Protocol. Front Oncol. 2021;11:617937.

57. Taves MD, Ashwell JD. Glucocorticoids in T cell development, differentiation and function. Nat Rev Immunol. aprile 2021;21(4):233–43.

58. Jing D, Huang Y, Liu X, Sia KCS, Zhang JC, Tai X, et al. Lymphocyte-Specific Chromatin Accessibility Pre-determines Glucocorticoid Resistance in Acute Lymphoblastic Leukemia. Cancer Cell. 10 dicembre 2018;34(6):906-921.e8.

59. Webster JC, Oakley RH, Jewell CM, Cidlowski JA. Proinflammatory cytokines regulate human glucocorticoid receptor gene expression and lead to the accumulation of the dominant negative β isoform: A mechanism for the generation of glucocorticoid resistance. Proceedings of the National Academy of Sciences of the United States of America. 29 maggio 2001;98(12):6865.

60. Kugler DG, Mittelstadt PR, Ashwell JD, Sher A, Jankovic D. CD4+ T cells are trigger and target of the glucocorticoid response that prevents lethal immunopathology in toxoplasma infection. J Exp Med. 23 settembre 2013;210(10):1919–27.

61. Elftman MD, Norbury CC, Bonneau RH, Truckenmiller ME. Corticosterone impairs dendritic cell maturation and function. Immunology. ottobre 2007;122(2):279.

62. Yang H, Xia L, Chen J, Zhang S, Martin V, Li Q, et al. Stress-glucocorticoid-TSC22D3 axis compromises therapy-induced antitumor immunity. Nat Med. settembre 2019;25(9):1428–41.

63. Piovan E, Yu J, Tosello V, Herranz D, Ambesi-Impiombato A, Da Silva AC, et al. Direct Reversal of Glucocorticoid Resistance by AKT Inhibition in Acute Lymphoblastic Leukemia. Cancer Cell. 9 dicembre 2013;24(6):766–76.

64. Bandapalli OR, Zimmermann M, Kox C, Stanulla M, Schrappe M, Ludwig WD, et al. NOTCH1 activation clinically antagonizes the unfavorable effect of PTEN inactivation in BFM-treated children with precursor T-cell acute lymphoblastic leukemia. Haematologica. giugno 2013;98(6):928–36.

65. Morishita N, Tsukahara H, Chayama K, Ishida T, Washio K, Miyamura T, et al. Activation of Akt is associated with poor prognosis and chemotherapeutic resistance in pediatric B-precursor acute lymphoblastic leukemia. Pediatr Blood Cancer. 15 luglio 2012;59(1):83–9.

66. Chiang MY, Xu L, Shestova O, Histen G, L'heureux S, Romany C, et al. Leukemia-associated NOTCH1 alleles are weak tumor initiators but accelerate K-ras-initiated leukemia. J Clin Invest. settembre 2008;118(9):3181–94.

67. Piovan E, Yu J, Tosello V, Herranz D, Ambesi-Impiombato A, Da Silva AC, et al. Direct reversal of glucocorticoid resistance by AKT inhibition in acute lymphoblastic leukemia. Cancer Cell. 9 dicembre 2013;24(6):766–76.

68. Brown JA, Ferrando A. Glucocorticoid Resistance in Acute Lymphoblastic Leukemia: BIM Finally. Cancer Cell. 10 dicembre 2018;34(6):869–71.

69. Meyer LK, Huang BJ, Delgado-Martin C, Roy RP, Hechmer A, Wandler AM, et al. Glucocorticoids paradoxically facilitate steroid resistance in T cell acute lymphoblastic leukemias and thymocytes. J Clin Invest. 3 febbraio 2020;130(2):863–76.

70. De Smedt R, Morscio J, Goossens S, Van Vlierberghe P. Targeting steroid resistance in T-cell acute lymphoblastic leukemia. Blood Rev. novembre 2019;38:100591.

71. Christensen SB, Andersen A, Poulsen JC, Treiman M. Derivatives of thapsigargin as probes of its binding site on endoplasmic reticulum Ca2+ ATPase. Stereoselectivity and important functional groups. FEBS Lett. 13 dicembre 1993;335(3):345–8.

72. Loewe S. The problem of synergism and antagonism of combined drugs. Arzneimittelforschung. giugno 1953;3(6):285–90.

73. Chou TC. Drug combination studies and their synergy quantification using the Chou-Talalay method. Cancer Res. 15 gennaio 2010;70(2):440–6.

74. Eberlé D, Hegarty B, Bossard P, Ferré P, Foufelle F. SREBP transcription factors: master regulators of lipid homeostasis. Biochimie. 1 novembre 2004;86(11):839–48.

75. Moore G, Annett S, McClements L, Robson T. Top Notch Targeting Strategies in Cancer: A Detailed Overview of Recent Insights and Current Perspectives. Cells. 20 giugno 2020;9(6):1503.

76. Chen B, Jiang L, Zhong ML, Li JF, Li BS, Peng LJ, et al. Identification of fusion genes and characterization of transcriptome features in T-cell acute lymphoblastic leukemia. Proc Natl Acad Sci U S A. 9 gennaio 2018;115(2):373–8.

77. Deangelo DJ, Stone RM, Silverman LB, Stock W, Attar EC, Fearen I, et al. A phase I clinical trial of the notch inhibitor MK-0752 in patients with T-cell acute lymphoblastic leukemia/lymphoma (T-ALL) and other leukemias. JCO. 20 giugno 2006;24(18_suppl):6585–6585.

78. Doody RS, Raman R, Sperling RA, Seimers E, Sethuraman G, Mohs R, et al. Peripheral and central effects of γ-secretase inhibition by semagacestat in Alzheimer's disease. Alzheimers Res Ther. 2015;7(1):36.

79. Roti G, Carlton A, Ross KN, Markstein M, Pajcini K, Su AH, et al. Complementary genomic screens identify SERCA as a therapeutic target in NOTCH1 mutated cancer. Cancer Cell. 18 marzo 2013;23(3):390–405.

80. Autzen HE, Siuda I, Sonntag Y, Nissen P, Møller JV, Thøgersen L. Regulation of the Ca(2+)-ATPase by cholesterol: a specific or non-specific effect? Mol Membr Biol. 2015;32(3):75–87.

81. Conrard L, Tyteca D. Regulation of Membrane Calcium Transport Proteins by the Surrounding Lipid Environment. Biomolecules. 20 settembre 2019;9(10):513.

8. FIGURE LEGENDS

Figure 1. CAD204520 Overcomes Thapsigargin Resistance in T-ALL

A) Crystal structure of the SERCA-CAD204520 complex. Right panel: cartoon and surface representation of SERCA (light blue) with CAD204520 bound at the membrane interface (orange surface representation). Left panels: close-up of the CAD204520 binding sites, as seen parallel to the membrane (upper panel) or along the membrane normal (lower panel). Dashed lines indicate polar interactions with Asp59 (2.9A°) and Asn101 (2.7A°). Nitrogen is shown in blue, oxygen in red, and fluorine in cyan. Carbon is light blue for SERCA and orange for CAD204520.

B) Simulated annealing omits map (green mesh) of CAD204520 (orange), contoured at 3.0 sigma. The top panel is viewed roughly along the membrane plane; the bottom panel, is viewed roughly perpendicular to the membrane.

C) Lollipop graphs showing sequenced mutations in the exonic region of ATP2A1, ATP2A2, and ATP2A3 genes. Allelic variants are depicted with a circle (black, synonymous; red, missense) relative to their amino acid position (gray bottom bar, aa) and to their protein domains (color coded). The length of the lollipop (number of mutations) bar indicates: if 0, no mutations occur; if 1, mutations occur in one sample; if 2, mutations occur in both samples.

D) Effect of CAD204520 and TG and CAD204520 treatment in parental and resistant ALL/SIL cells lines. Histograms show percentage of cells alive after 72 h of treatment at the indicated concentrations (~IC50). Error bar denotes the mean ± SD of a minimum of three replicates. Statistical significance among groups (****p % 0.0001) was determined by one-way ANOVA.

E) Surface plots analysis of ALL/SIL, DND41, and RPMI-8402 T-ALL cell lines treated with vehicle, CAD204520, TG, or CAD204520 plus TG. Each point represents an independent

measurement representative of three biological replicates. Plots were generated using the Combenefit script by MATLAB R201, which represents the Loewe (dose-effect-based approach) analysis. A color scale bar represents the level of drug antagonism or synergism. F) Combination index analysis for the combinations of CAD204520 with TG in ALL/SIL, DND41 and RPMI-8402 T-ALL cell lines *NOTCH1*- mutated T-ALL treated for 3 days. On the y axis is represented the combination index, on the x axis the fraction of cells inhibited.

Figure 2. Transcriptomic profiling highlights increased steroid metabolism

A) Gene expression heatmap of the top 500 differentially expressed genes in ALL/SIL R (red) vs ALL/SIL (blue) filtered by adjusted p-value (<0.05) and log2 Fold Change (>1). The top half clearly shows genes with higher expression (from yellow to red) in ALL/SIL R cells while the bottom half shows the opposite scenario.

B) Volcano plot of the top differentially expressed genes (adjusted p-value threshold = 1e-20, horizontal dashed line; log2 Fold Change threshold of 1, vertical dashed line) in ALL/SIL R vs ALL/SIL. Genes in red are up-regulated in ALL/SIL R cells while genes in blue are down-regulated.

C) Network visualization of the most interesting pathways resulting from GSEA. The graph illustrated these relationships, where nodes commonly represent specific pathways or genes, such as those involved in cholesterol biosynthesis, with each step corresponding to enzymes and reactions contributing to cholesterol production. Edges or lines between nodes indicate functional connections, such as shared molecules or regulatory influences between pathways. Clusters of nodes signify closely related or co-regulated pathways, as often seen with lipid biosynthesis and cholesterol metabolism. These clusters help reveal pathways that are co-dependent, governed by common regulatory mechanisms, or affected by shared signaling molecules. Pathway nodes size is proportional to the number of genes they contain. Gene nodes are colored by log2 Fold Change derived from DE.

D) Barplot of top Transcription factors enriched/depleted in ALL/SIL R compared to ALL/SIL. Each TF is ranked by Normalized Enrichment Score (NES) computed using the wald statistics from the differential analysis.

E) Barplot of Pathway activity inferred using PROGENy. Pathways in red are more active in ALL/SIL R while blue ones are more active in ALL/SIL. Each pathway is ranked by NES, which is estimated with a permutation approach.

Figure 3. GC sensitivity in *NOTCH1*-mutated TG-resistant cells with *ATP2A2* mutation

A) Radar plots reporting drug screening results in ALL/SIL (blue lines) and ALL/SIL R (red lines) cell lines, in terms of cell viability reduction. All reported results were obtained considering a drug concentration equal to 100 nM. The radar plot shows the effect of specific drug subgroups in both cell lines: compounds that cause a viability reduction under 50% in both cell lines.

B) Radar plots reporting drug screening results in ALL/SIL (blue lines) and ALL/SIL R (red lines) cell lines, in terms of cell viability reduction. All reported results were obtained considering a drug concentration equal to 100 nM. The radar plot shows the effect of specific drug subgroups in both cell lines: compounds that cause a viability reduction only in ALL/SIL (bottom right).

C) Radar plots reporting drug screening results in ALL/SIL (blue lines) and ALL/SIL R (red lines) cell lines, in terms of cell viability reduction. All reported results were obtained considering a drug concentration equal to 100 nM. The radar plot shows the effect of specific drug subgroups in both cell lines: compounds that cause a viability reduction only in ALL/SIL R.

D) Radar plot showing the highest-ranked classes of small molecules that are distinctly active in the resistant cell lines. Among these, there are GCs (dexamethasone, clobetasol propionate, and fluticasone propionate) which modulate nuclear receptor activity.

Figure 4. *ATP2A2* mutation restores GR function, promoting synergy with GCs and SERCA inhibitors

A) Immunoblotting showing expression of Notch1 pathway and total GR in T-ALL cell lines.

B) Immunoblotting showing expression of Notch1 pathway and total GR in T-ALL R cell lines. Real-time PCR results comparing the fold change in gene expression of GCs receptor in ALL/SIL, ALL/SIL R, MOLT4, MOLT4 R cell lines in basal conditions. The y axis represents the fold change between each condition and β-actin expression as an internal control. Error bar denotes the mean ± SD of a minimum of three replicates. Statistical significance among groups (*P < 0.05, ****P < 0.0001) was determined by one-way ANOVA.

C) Effects of GCs on cell viability after 72 hours of treatments in T-ALL cell lines. Error bars denote ± SD of 3 replicates.

D) Effects of GCs on cell viability after 72 hours of treatments in T-ALL cell lines in basal conditions and after rescue with ALL/SIL R media. Error bars denote ± SD of 2 replicates. Black: rescue conditions; Rose: basal conditions

E) Effects of GCs on cell viability in ALL/SIL and ALL/SIL R T-ALL cell lines with the following conditions: after 72 hours of treatments, after 72 hours of treatments in combination with TG 10 nM; after a pre-treatment with RU486 1 μM and TG 10 nM for 24 hours and a following treatment with GCs for 72 hours. Error bars denote ± SD of 2 replicates.

F) Surface plots analysis of ALL/SIL, ALL/SIL R T-ALL cell lines treated with dexamethasone, clobetasol propionate or fluticasone propionate plus CAD204520. Each point represents an independent measurement representative of three biological replicates. Plots were generated using the Combenefit script by MATLAB R201, which represents the Loewe (dose-effect-based approach) analysis. A color scale bar represents the level of drug antagonism or synergism.

G) Combination index analysis for the combinations of CAD204520 with dexamethasone, clobetasol proprionate or fluticasone propionate in ALL/SIL and ALL/SIL R T-ALL cell lines

treated for 3 days. On the y axis is represented the combination index, on the x axis the fraction of cells inhibited.

Figure 5. SERCA mutant cells cluster within the TAL/LMO genetic subgroup

A) The heatmap shows the OncoPrint distribution of genetic alterations across key signaling pathways in T-ALL samples. Rows represent individual genes, and columns correspond to patient samples. Black squares indicate the presence of genetic alterations. Genes are grouped by pathway involvement, denoted by the color-coded bar on the left of the heatmap: transcriptional regulation (brown), JAK-STAT (blue), PI3K-AKT (light green), RAS (red), and Notch signaling (green).The histograms above each column represent the SilR Score (log2 (TMP+1)) per patient sample, with the lowest 10th percentile shown in blue and the top 10th percentile in red. The histogram on the right shows the percentage of each gene mutation across the dataset. The bars below the heatmap represent genetic subtype: LM02/LYL1, HOXA, TLX3, TLX1, NKX2-1, LMO1/2, TAL1, TAL2, and Unknown.

B) Analysis of T-ALL genetic subgroups based on SilR score. High score: greater similarity to the ALLSIL R signature. Low score: greater similarity to the ALLSIL signature.

C) Bar plot showing T-ALL primary samples collected and classified according to their genetic subgroup.

D) T-ALL primary samples from the TAL/LMO genetic subgroup. Table shows the IC50 (μM) and AUC values for CAD204520, Dexamethasone and their combined therapy.

Figure 6. GC and CAD204520 combination show anti-leukemia activity in TAL1-rearranged T-ALL model *in vivo*

A) Schematic representation of the experiment.

B) Antileukemic activity of dexamethasone and CAD204520 in hCD45+ T-ALL leukemia cells (peripheral blood) in a PDLX T-ALL murine model after 21 days of treatment

(CAD204520: 30 mg/kg/os BID, dexamethasone: 5 mg/kg/IP) or vehicle (PBS). Error bar denotes the mean ± SD of a minimum of eight replicates. Statistical significance for treated vs. vehicle (***P < 0.001) was determined by non-parametric t-test (Mann–Whitney).

C) Antileukemic activity of dexamethasone and CAD204520 in hCD45+ T-ALL leukemia cells (bone marrow) in a PDLX T-ALL murine model after 21 days of treatment (CAD204520: 30 mg/kg/os BID, dexamethasone: 5 mg/kg/IP) or vehicle (PBS). Error bar denotes the mean ± SD of a minimum of eight replicates. Statistical significance for treated vs. vehicle (***P < 0.001) was determined by non-parametric t-test (Mann–Whitney).

D) Effect of CAD204520 and dexamethasone on spleen size after 21 days of treatment. Error bar denotes the mean ± SD of a minimum of eight replicates. Statistical significance for treated vs. vehicle (***P < 0.001) was determined by non-parametric t-test (Mann–Whitney).

E) Histograms show the effect of daily 30 mg/kg administration of CAD204520 and 5 mg/Kg of dexamethasone on body weight. Error bar denotes the mean ± SD of a minimum of seven replicates. Statistical significance among groups (*P < 0.05, ****P < 0.0001) was determinated by a two-way ANOVA with Sidak's multiple comparisons testing.

F) CD45 expression in bone marrow leukemia cells (PDLX T-ALL murine model) following 21 days treatment (CAD204520: 30 mg/kg/os BID, dexamethasone: 5 mg/kg/IP). Bone marrow of all mice was examined; representative results for one control animal and one CAD204520 or Dexamethasone-treated animal are shown. FFPE tissues were stained with hCD45. Scale bars, 100 μm.

G) Histograms display the mean ±SD of the percentage of the CD45-positive cells in FFPE tissue sections. Error bar denotes the mean ± SD of a minimum of thirteen replicates. Statistical significance among groups (****P < 0.0001) was determinated by non-parametric t-test (Mann–Whitney).

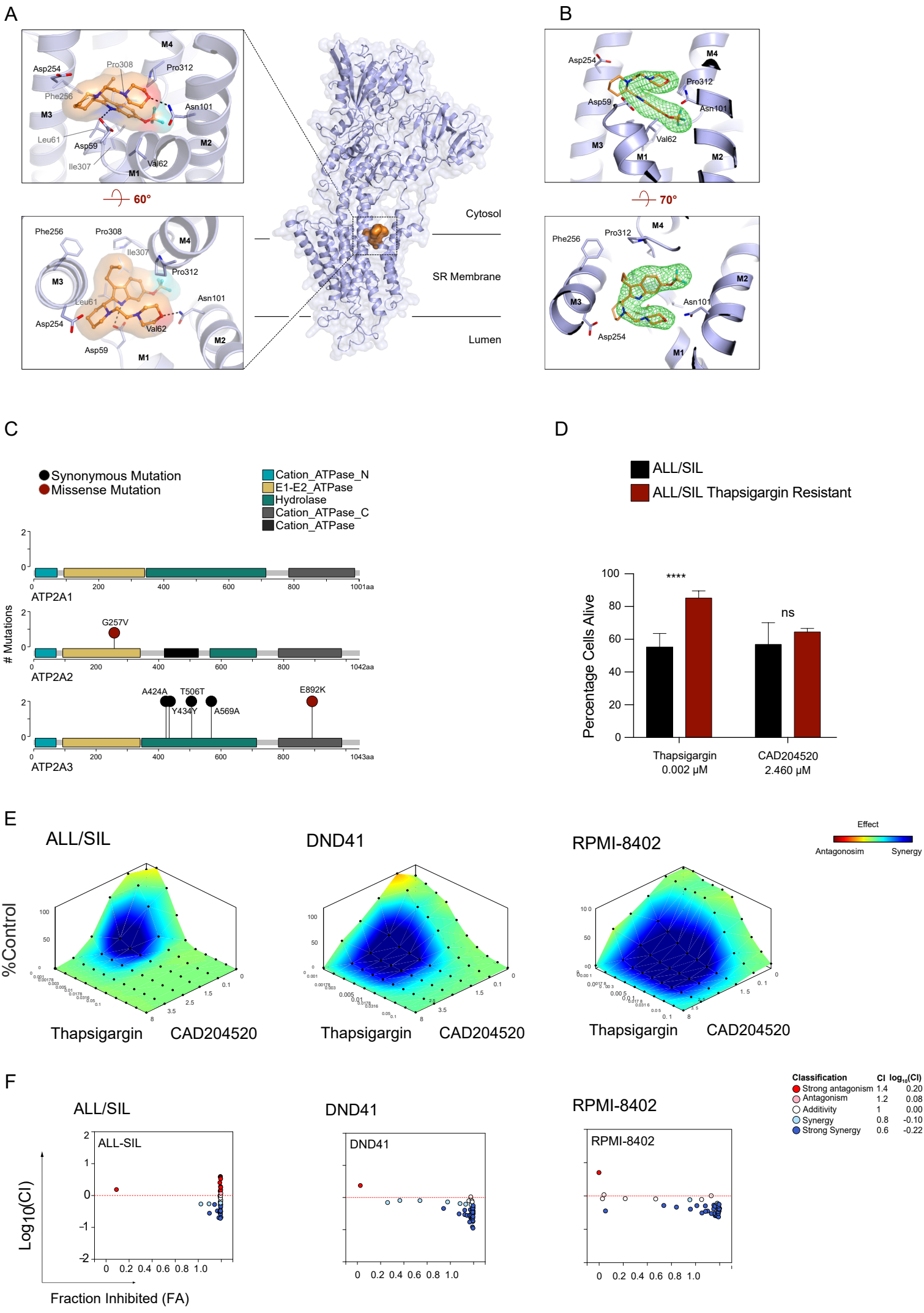
A
M4
Asp254
Pro308
Pro312
Phe256
Asn101
M3
Leu61
Asp59
M2
Ile307
Val62
M1
60°
Phe256
Pro308
M4
Ile307
Pro312
M3
Leu61
Asn101
Asp254
Val62
Asp59
M2
M1
Cytosol
SR Membrane
Lumen
B
Asp254
M4
Pro312
Asp59
Asn101
Val62
M3
M1
M2
70°
Phe256
Pro312
M4
M2
M3
Asn101
Asp254
M1
C
Synonymous Mutation
Missense Mutation
Cation_ATPase_N
E1-E2_ATPase
Hydrolase
Cation_ATPase_C
Cation_ATPase
Mutations
ATP2A1
ATP2A2
G257V
ATP2A3
A424A
T506T
Y434Y
A569A
E892K
D
ALL/SIL
ALL/SIL Thapsigargin Resistant
Percentage Cells Alive
****
ns
Thapsigargin
0.002 μM
CAD204520
2.460 μM
E
ALL/SIL
DND41
RPMI-8402
Effect
Antagonosim
Synergy
%Control
Thapsigargin
CAD204520
F
ALL/SIL
DND41
RPMI-8402
Classification
CI
log10(CI)
Strong antagonism 1.4 0.20
Antagonism 1.2 0.08
Additivity 1 0.00
Synergy 0.8 -0.10
Strong Synergy 0.6 -0.22
Log10(CI)
Fraction Inhibited (FA)

Figure 1

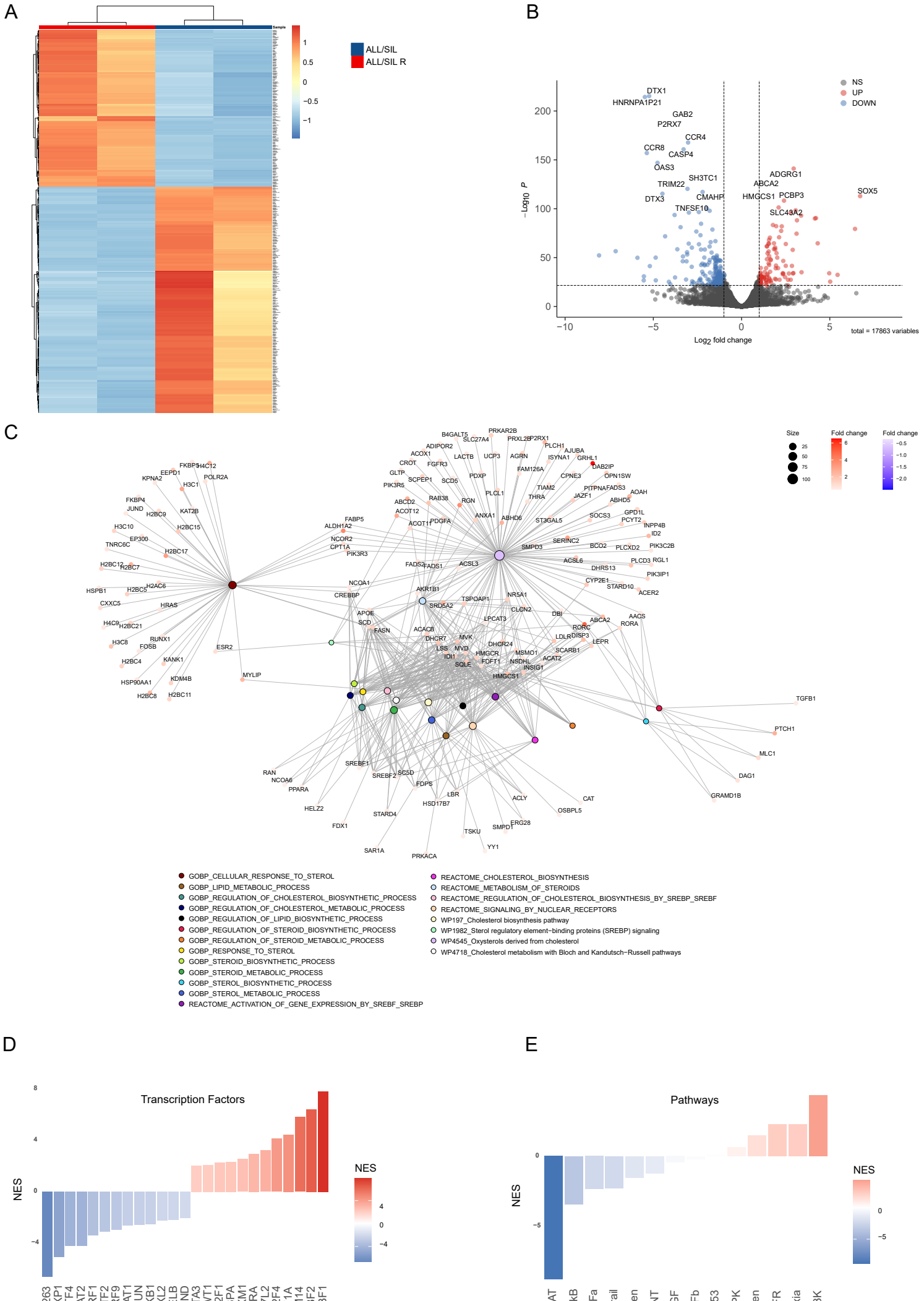
A
ALL/SIL
ALL/SIL R
B
NS
UP
DOWN
DTX1
HNRNPA1P21
GAB2
P2RX7
CCR4
CCR8
CASP4
OAS3
TRIM22
DTX3
SH3TC1
CMAHP
TNFSF10
ADGRG1
ABCA2
HMGCS1
PCBP3
SLC43A2
SOX5
−Log10 P
Log2 fold change
total = 17863 variables
C
Size
Fold change
Fold change
GOBP_CELLULAR_RESPONSE_TO_STEROL
GOBP_LIPID_METABOLIC_PROCESS
GOBP_REGULATION_OF_CHOLESTEROL_BIOSYNTHETIC_PROCESS
GOBP_REGULATION_OF_CHOLESTEROL_METABOLIC_PROCESS
GOBP_REGULATION_OF_LIPID_BIOSYNTHETIC_PROCESS
GOBP_REGULATION_OF_STEROID_BIOSYNTHETIC_PROCESS
GOBP_REGULATION_OF_STEROID_METABOLIC_PROCESS
GOBP_RESPONSE_TO_STEROL
GOBP_STEROID_BIOSYNTHETIC_PROCESS
GOBP_STEROID_METABOLIC_PROCESS
GOBP_STEROL_BIOSYNTHETIC_PROCESS
GOBP_STEROL_METABOLIC_PROCESS
REACTOME_ACTIVATION_OF_GENE_EXPRESSION_BY_SREBF_SREBP
REACTOME_CHOLESTEROL_BIOSYNTHESIS
REACTOME_METABOLISM_OF_STEROIDS
REACTOME_REGULATION_OF_CHOLESTEROL_BIOSYNTHESIS_BY_SREBP_SREBF
REACTOME_SIGNALING_BY_NUCLEAR_RECEPTORS
WP197_Cholesterol biosynthesis pathway
WP1982_Sterol regulatory element−binding proteins (SREBP) signaling
WP4545_Oxysterols derived from cholesterol
WP4718_Cholesterol metabolism with Bloch and Kandutsch−Russell pathways
D
Transcription Factors
NES
ZNF263
FOXP1
ATF4
STAT2
IRF1
ATF2
IRF9
STAT1
JUN
NFKB1
FOXL2
RELB
JUND
GATA3
WT1
E2F1
CEBPA
FOXM1
PPARA
TCF7L2
E2F4
HIF1A
PRDM14
SREBF2
SREBF1
E
Pathways
NES
JAK.STAT
NFkB
TNFa
Trail
Estrogen
WNT
VEGF
TGFb
p53
MAPK
Androgen
EGFR
Hypoxia
PI3K

Figure 2

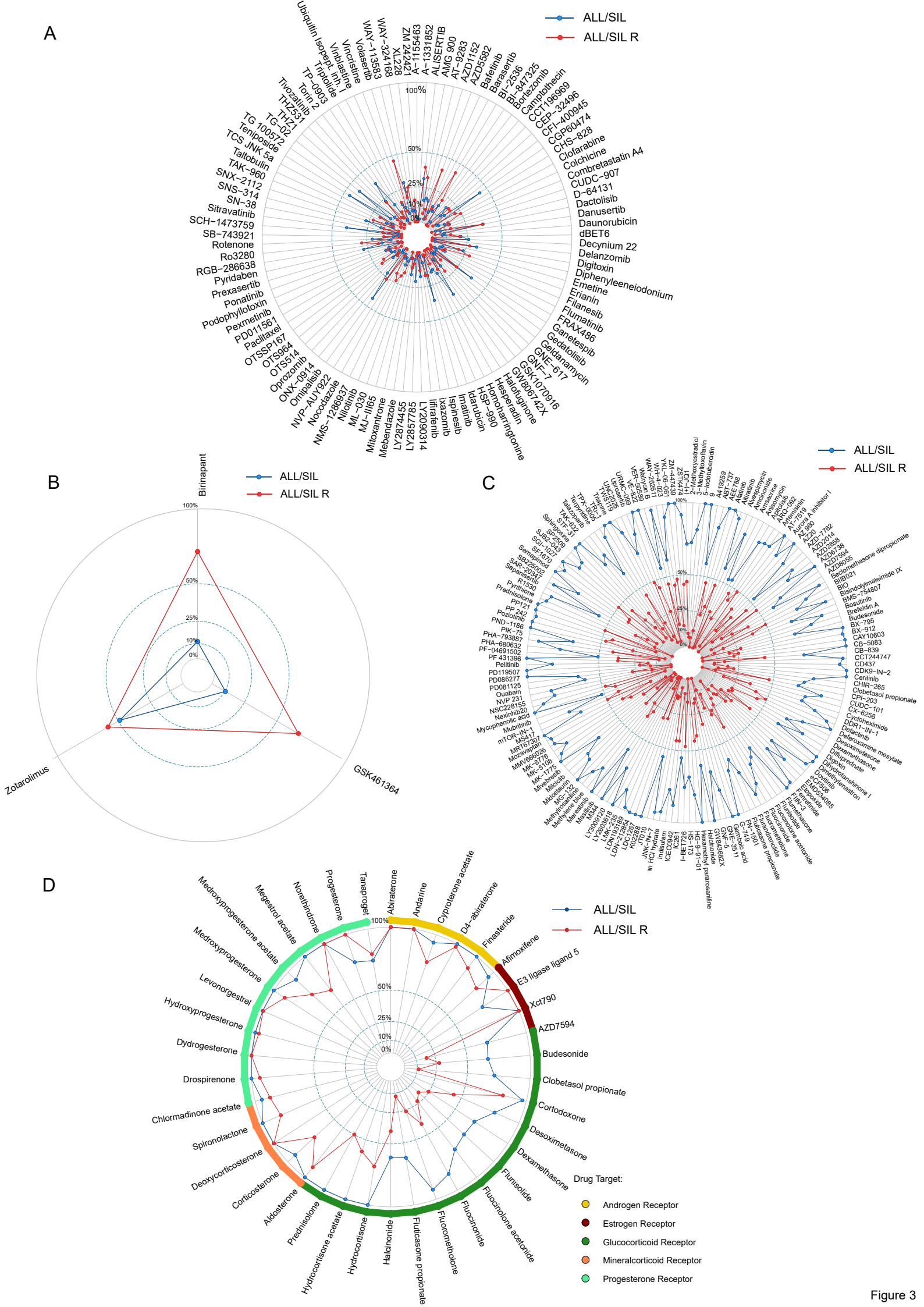
A
ALL/SIL
ALL/SIL R
B
Birinapant
Zotarolimus
GSK461364
C
D
Drug Target:
Androgen Receptor
Estrogen Receptor
Glucocorticoid Receptor
Mineralcorticoid Receptor
Progesterone Receptor

Figure 3

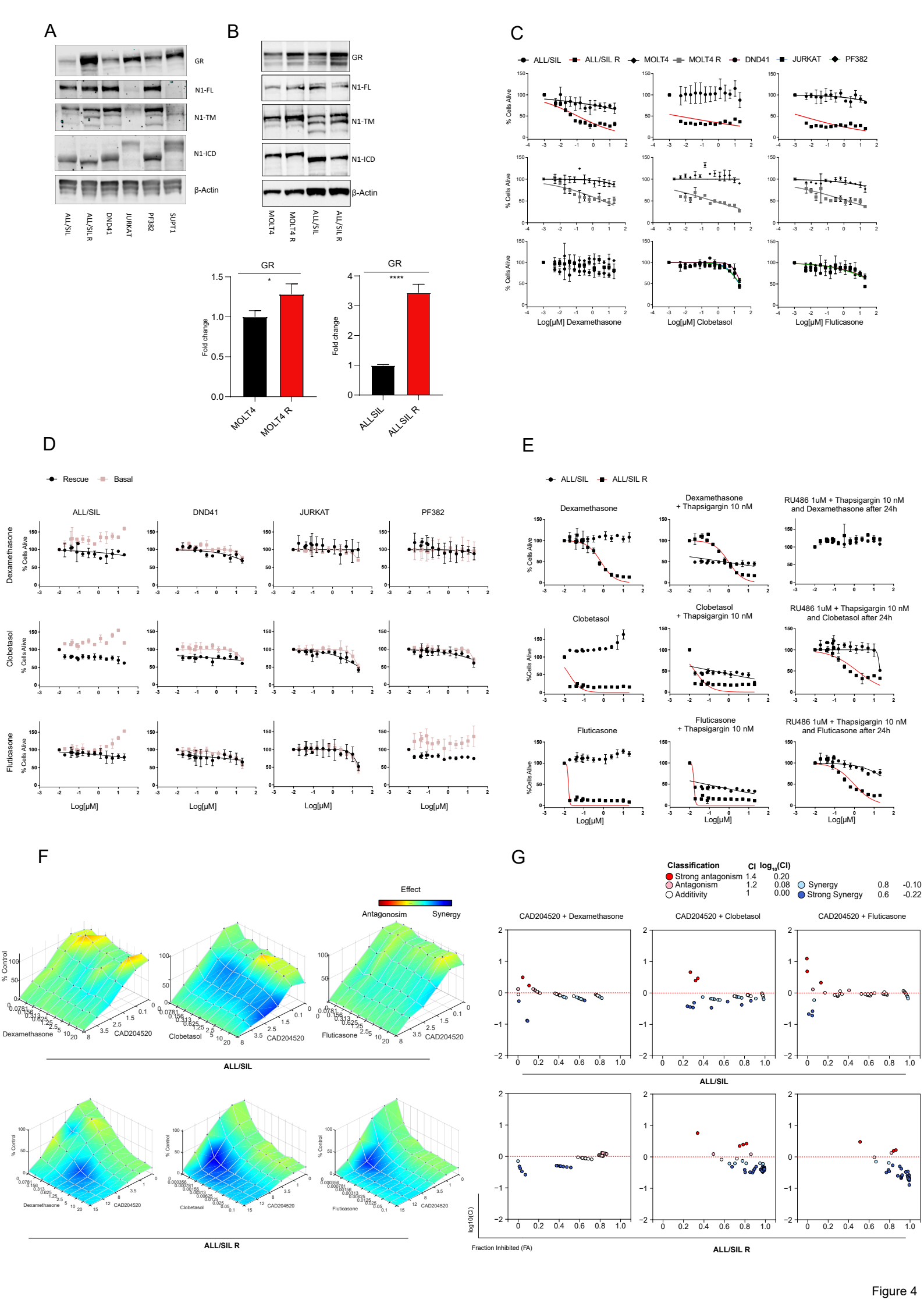
A
GR
N1-FL
N1-TM
N1-ICD
β-Actin
ALL/SIL
ALL/SIL R
DND41
JURKAT
PF382
SUPT1
B
GR
N1-FL
N1-TM
N1-ICD
β-Actin
MOLT4
MOLT4 R
ALL/SIL
ALL/SIL R
GR
*
Fold change
MOLT4
MOLT4 R
GR
****
Fold change
ALLSIL
ALLSIL R
C
ALL/SIL
ALL/SIL R
MOLT4
MOLT4 R
DND41
JURKAT
PF382
% Cells Alive
Log[μM] Dexamethasone
Log[μM] Clobetasol
Log[μM] Fluticasone
D
Rescue
Basal
ALL/SIL
DND41
JURKAT
PF382
Dexamethasone
Clobetasol
Fluticasone
% Cells Alive
Log[μM]
E
ALL/SIL
ALL/SIL R
Dexamethasone
Dexamethasone + Thapsigargin 10 nM
RU486 1uM + Thapsigargin 10 nM and Dexamethasone after 24h
Clobetasol
Clobetasol + Thapsigargin 10 nM
RU486 1uM + Thapsigargin 10 nM and Clobetasol after 24h
Fluticasone
Fluticasone + Thapsigargin 10 nM
RU486 1uM + Thapsigargin 10 nM and Fluticasone after 24h
% Cells Alive
Log[μM]
F
Effect
Antagonosim
Synergy
% Control
Dexamethasone
Clobetasol
Fluticasone
CAD204520
ALL/SIL
ALL/SIL R
G
Classification
CI
log10(CI)
Strong antagonism 1.4 0.20
Antagonism 1.2 0.08
Additivity 1 0.00
Synergy 0.8 -0.10
Strong Synergy 0.6 -0.22
CAD204520 + Dexamethasone
CAD204520 + Clobetasol
CAD204520 + Fluticasone
ALL/SIL
ALL/SIL R
log10(CI)
Fraction Inhibited (FA)

Figure 4

A

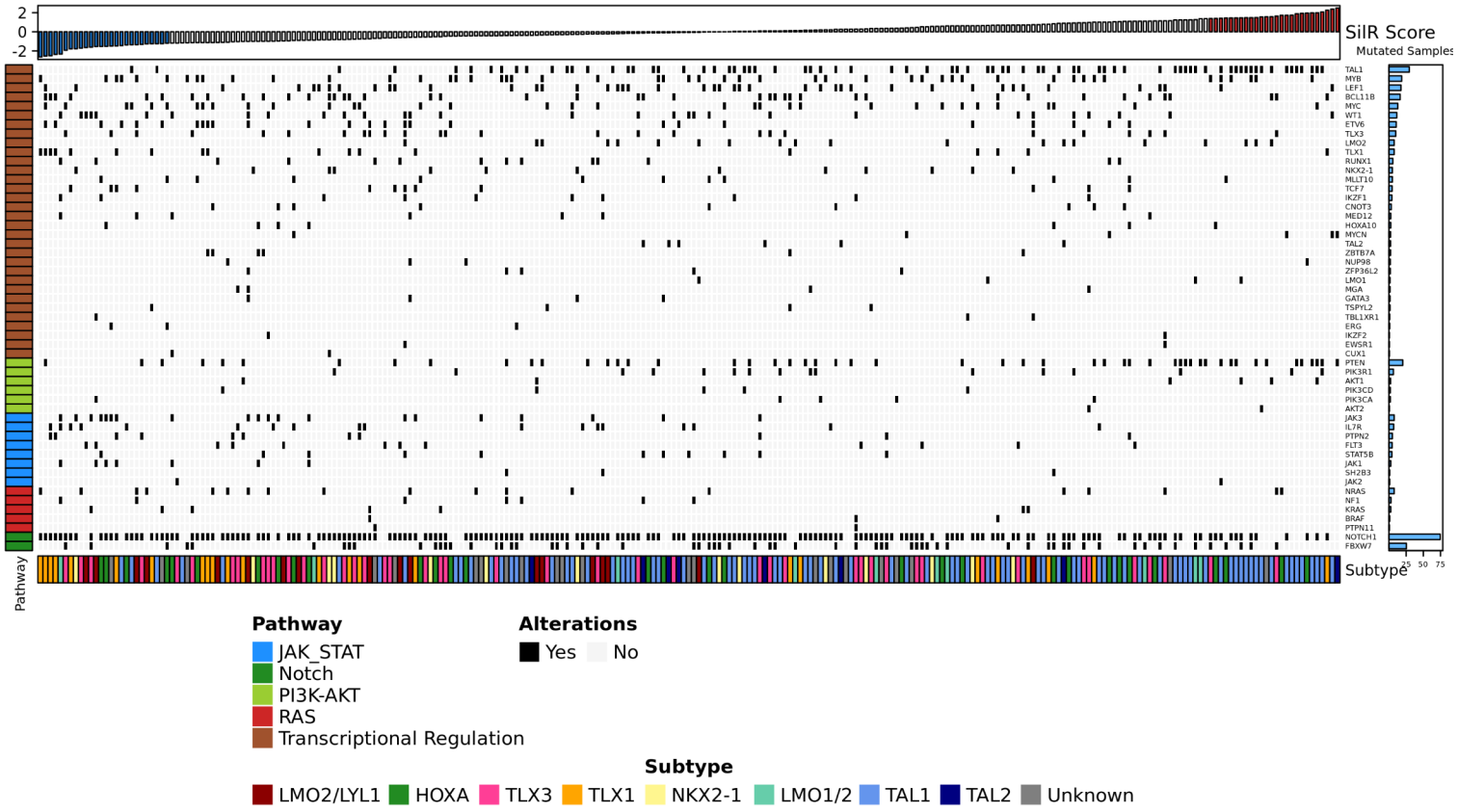

B

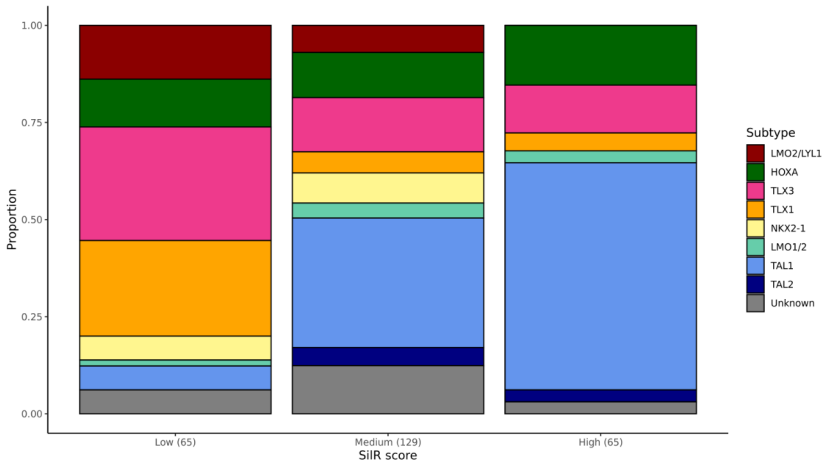

C

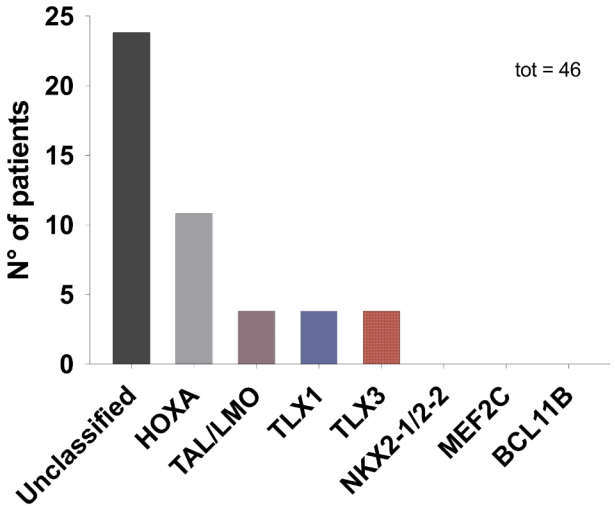

D

Patient	Sex	Phenotype	CI-FISH	IC50 (µM) / AUC		
				CAD	Dex	CAD+Dex
BM-117-2021	M	Early	STIL::TAL1 CDKN2AB bDEL CASP8AP2-GRIK2-SEC63-FYN del NF1-SUZ12 gain TP53 DEL	8.59 365	NR 295	0.85 263
BM-122-2021	M	Early	SIL::TAL1 NF1 del SUZ2 del	5.59 343	0.27 215	0.06 189
BM-015-2021	M	Mature	TRAD::LMO2 CDKN2AB del GRIK2-CASP8AP2-SEC63-FYN del TP53 mDEL	1.58 304	NR 350	1.94 290
BM-066-2022	F	Pro-T/ETP	TRAD::LMO2; LEF1 del; iso(17q)/TP53del	4.01 336	0.03 165	0.02 153

Figure 5

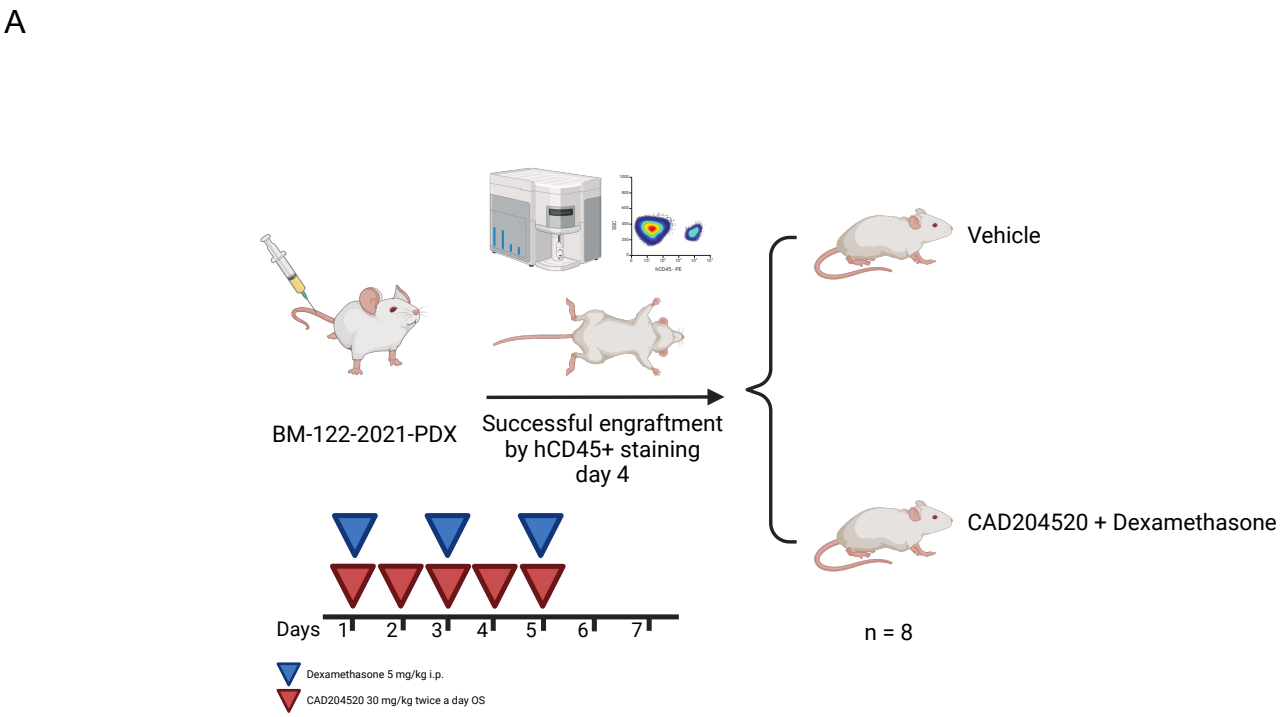
A
Vehicle
BM-122-2021-PDX
Successful engraftment
by hCD45+ staining
day 4
CAD204520 + Dexamethasone
n = 8
Days 1 2 3 4 5 6 7
Dexamethasone 5 mg/kg i.p.
CAD204520 30 mg/kg twice a day OS

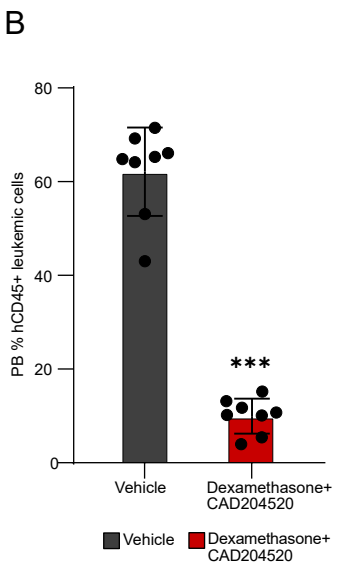
B
PB % hCD45+ leukemic cells
80
60
40
20
0
***
Vehicle
Dexamethasone+
CAD204520
Vehicle
Dexamethasone+
CAD204520

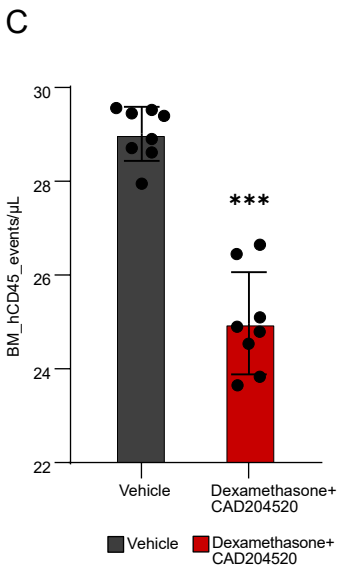
C
BM_hCD45_events/µL
30
28
26
24
22
***
Vehicle
Dexamethasone+
CAD204520
Vehicle
Dexamethasone+
CAD204520

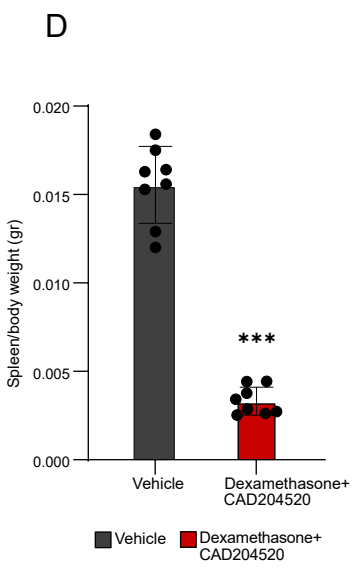
D
Spleen/body weight (gr)
0.020
0.015
0.010
0.005
0.000
***
Vehicle
Dexamethasone+
CAD204520
Vehicle
Dexamethasone+
CAD204520

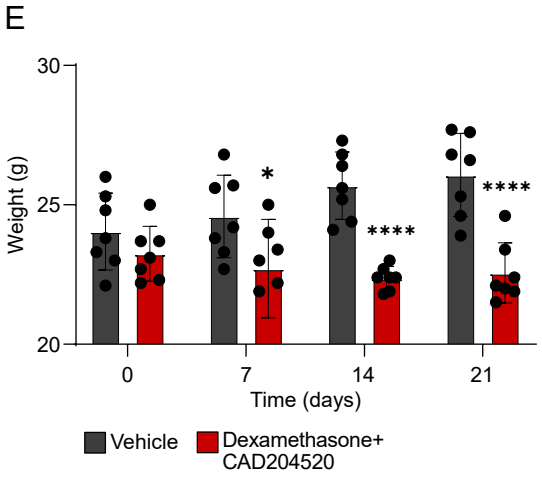
E
Weight (g)
30
25
20
0
7
14
21
Time (days)
*
****
****
Vehicle
Dexamethasone+
CAD204520

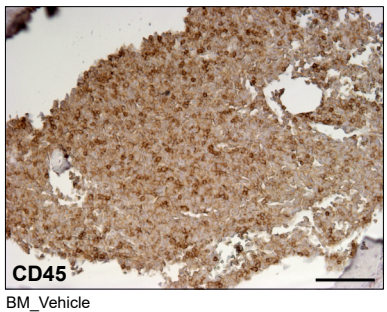
F
CD45
BM_Vehicle

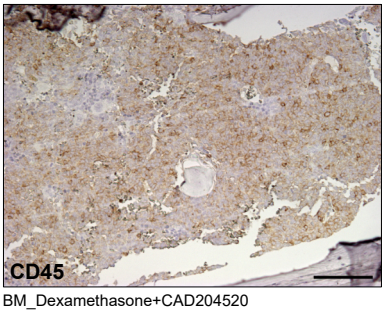
CD45
BM_Dexamethasone+CAD204520

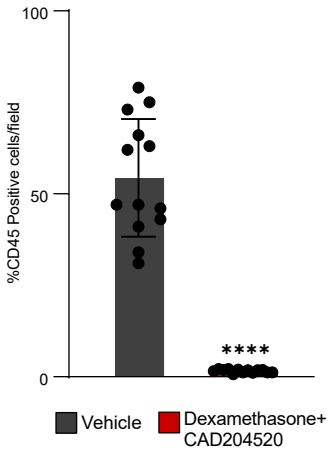
G
%CD45 Positive cells/field
100
50
0
****
Vehicle
Dexamethasone+
CAD204520

Figure 6